VOLUME 32 OCTOBER 1954 NUMBER 10

Canadian Journal of Physics

Published by THE NATIONAL RESEARCH COUNCIL
OTTAWA CANADA

CANADIAN JOURNAL OF PHYSICS

(Formerly Section A, Canadian Journal of Research)

Under the authority of the Chairman of the Committee of the Privy Council on Scientific and Industrial Research, the National Research Council issues annually THE CANADIAN JOURNAL OF PHYSICS and six other journals devoted to the publication of the results of original scientific research. Matters of general policy concerning these journals are the responsibility of a joint Editorial Board consisting of: members representing the National Research Council of Canada; the Editors of the Journals; and members representing the Royal Society of Canada and four other scientific societies.

Manuscripts for publication should be submitted to Dr. Léo Marion, Editor-in-Chief, Canadian Journal of Physics, National Research Council, Ottawa 2, Canada.
(For instructions on preparation of copy, see **Notes to Contributors** (inside back cover).)

Proof, correspondence concerning proof, and *orders for reprints* should be sent to the Manager, Editorial Office (Research Journals), Division of Administration, National Research Council, Ottawa 2, Canada.

Subscriptions, renewals, and orders for single or back numbers should be sent to Division of Administration, National Research Council, Ottawa 2, Canada. Remittances should be made payable to the Receiver General of Canada, credit National Research Council.

The journals published, frequency of publication, and prices are:

Canadian Journal of Biochemistry and Physiology	Bimonthly	$3.00 a year
Canadian Journal of Botany	Bimonthly	$4.00 a year
Canadian Journal of Chemistry	Monthly	$5.00 a year
Canadian Journal of Microbiology*	Bimonthly	$3.00 a year
Canadian Journal of Physics	Monthly	$4.00 a year
Canadian Journal of Technology	Bimonthly	$3.00 a year
Canadian Journal of Zoology	Bimonthly	$3.00 a year

The price of single numbers of all journals is 75 cents.

*Volume 1 will combine three numbers published in 1954 with six published in 1955 and will be available at the regular annual subscription rate of $3.00.

Canadian Journal of Physics

Issued by THE NATIONAL RESEARCH COUNCIL OF CANADA

VOLUME 32 OCTOBER 1954 NUMBER 10

THE ANGULAR DISTRIBUTION OF THE $Li^7(t, \alpha)He^6$ REACTIONS AT 240 KEV. TRITON ENERGY[1]

BY E. ALMQVIST, T. P. PEPPER,[2] AND P. LORRAIN[3]

ABSTRACT

The angular distributions of the $Li^7(t, \alpha)He^6$ reactions have been measured between 41° and 139° to the beam in the laboratory system. The distribution of the 5.95 Mev. α-particles associated with the formation of ground state He^6 is of the form $1 - 0.66(\pm 0.06)\cos^2\phi$ in the center of mass system. The 4.95 Mev. α-particles associated with the formation of the first excited state of He^6 are distributed isotropically within $\pm 8\%$. These results are consistent with the expectation that the ground state of He^6 has spin 0 and the first excited state spin 2 and suggest that the compound state, Be^{10}, has $J = 2$.

INTRODUCTION

The only *exothermic* charged particle reaction in which the nuclide He^6 has been observed as a product is produced by the bombardment of lithium with tritons. The study of this reaction, therefore, may be expected to yield new information about the properties and levels of He^6. Already investigations of the α-particle energy distribution at 90° to the triton beam have revealed an excited state of He^6 and have provided data permitting an accurate determination of the mass of this nucleus (6). These investigations have been extended to other angles, and this paper reports measurements made of the angular distributions of the $Li^7(t, \alpha)He^6$ reactions at 240 kev. bombarding energy.

In Fig. 1 is shown the energy distribution of α-particles emitted at 90° to a beam of tritons bombarding a target of Li^7. Most of the disintegrations result in a broad continuum of α-particles from the various multibody modes of breakup that are possible. There are, however, two sharp groups, one at 5.95 Mev. and one at 4.95 Mev. These α-particle groups are identified with the reactions:

(i) $Li^7 + T \rightarrow He^6 + He^4 + 9.79$ Mev.,

(ii) $Li^7 + T \rightarrow He^{6*} + He^4 + 8.08$ Mev.,

which yield He^6 in the ground state and an excited state respectively. This excited state lies 1.71 Mev. above the ground state and is unstable by 0.78 Mev. against breakup into an α-particle and two neutrons (6).

[1]*Manuscript received July 14, 1954.*
Contribution from Atomic Energy of Canada Limited, Chalk River, Ontario. Issued as A.E.C.L. No. 129.
[2]*Now with Isotope Products Limited, Oakville, Ontario.*
[3]*Permanent address: Université de Montréal, Montreal, P.Q.*

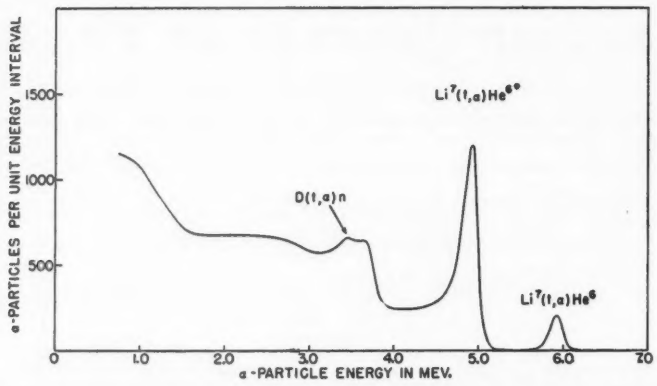

FIG. 1. The energy distribution of α-particles emitted at 90° to a beam of tritons bombarding a target of Li^7.

EXPERIMENTAL ARRANGEMENT

Hydrogen containing 65% tritium was used in the ion source of the Chalk River 250 kv. accelerator (1). The mass three beam was selected by a "straight through" analyzer which combines electrostatic deflection with magnetic deflection so that the emergent beam is parallel to the incident beam. The bombarding particles enter the target chamber vertically as shown in Fig. 2.

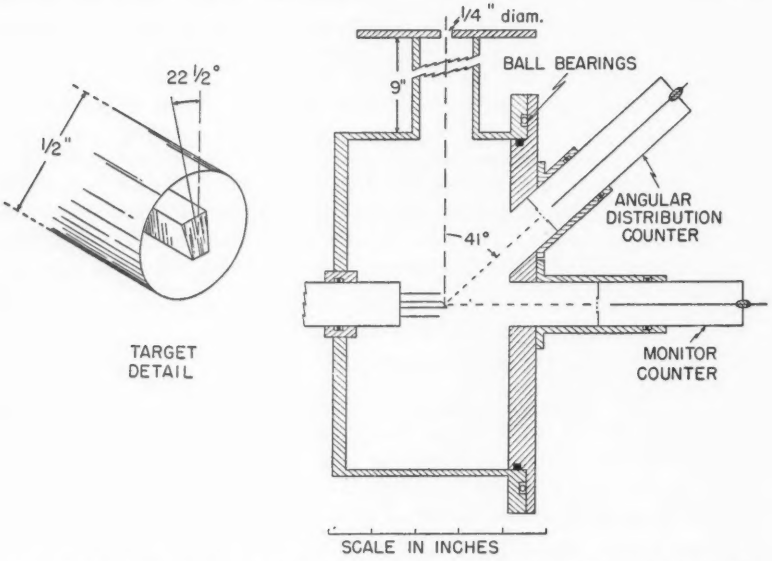

FIG. 2. Schematic diagram of the angular distribution chamber. An enlarged view of the target is shown at the left.

The target is made from $\frac{1}{8} \times \frac{1}{8}$ in. rectangular steel bar that is mounted on the axis of the chamber and at right angles to the beam. The target face is cut to make an angle of $22\frac{1}{2}°$ to the beam and the sides of the target are undercut by 7° so that they cannot be bombarded. A cylindrical stainless steel shield surrounds the stem of the target; thus only the face is visible to the beam. The angle between the axis of the target chamber and the beam is defined to $90° \pm 1°$ by the small size of the target and the $\frac{1}{4}$ in. aperture through which the beam enters the target chamber.

Two end window counters are mounted on a plate which rotates about the axis of the chamber. This plate rests on ball bearings and can easily be turned to any desired position while the system is evacuated. One counter, mounted on the center of the plate, remains always at 90° to the beam and is used to monitor the yield. The output from this counter after suitable amplification is fed to a discriminator; and pulses larger than a chosen value are counted. A second counter is placed at an angle of 49° to the axis of the chamber and can thus be set to make any desired angle between 41° and 139° to the beam by rotating the mounting plate. The output from this counter is amplified and displayed on a 30-channel pulse height analyzer in order to allow the α-particle groups to be distinguished and observed separately at each angle. The geometry is such that only particles deviating by less than $\pm 3°$ from the angle between the beam and the center line of the counter are detected.

THE COUNTERS

The end window proportional counters are made of $1\frac{1}{8}$ in. I.D. copper tube with a central electrode of 0.008 in. tungsten wire. One end of this is brought out through a polythene insulator and the other end is left free but terminated $\frac{1}{4}$ in. from the mica window by a small glass bead about 1/32 in. in diameter. Counters of this type, up to 4 in. long, showed less than a millimeter sag of the bead when held horizontally, and operated satisfactorily. As far as possible the counters were maintained with the same side up so that the position of the bead would not change with angle. This was done as a precaution although no change in the effective aperture of the counters due to the slight motion of the bead was detected.

Alpha particles up to 8.5 Mev. energy could be stopped in the sensitive volume of the counter when it was filled to 68 cm. pressure with argon containing 5% carbon dioxide and equipped with a 2.6 mgm./cm.^{2} mica window. A thinner window of 1.5 mgm./cm.^{2} of mica was used to repeat some of the measurements at angles greater than 90° where the forward motion of the center of mass reduces the particle energies.

Since the reaction $D(t, \alpha)n$ always occurs when low energy tritons are accelerated and the intensity varies with target conditions (2), it is essential that the monitor does not count the resultant 3.5 Mev. α-particles. This condition is achieved by equipping the monitor counter with a 3.0 mgm./cm.^{2} window. The 8.7 Mev. α-particles produced by the protons in the beam reacting with Li^7 cannot be excluded by the thick window. However, their intensity can be determined in the angular distribution counter where a pulse height spectrum is taken. This measured intensity together with the data

obtained from angular distribution measurements of the $Li^7(p, \alpha)He^4$ reaction can be used to compute the number of these α-particles that are counted in the monitor, and a correction can accurately be made. This correction amounted to less than 6% in each case.

THE TARGETS

The earlier work (6, 8) with separated isotopes has shown that the yield of α-particles from the Li^6 isotope in natural lithium is negligible at 240 kev. bombarding energy compared with that from Li^7. Hence natural lithium fluoride targets were used for the angular distribution measurements. The targets were prepared by placing a small quantity of lithium fluoride on the target face and then heating the back of the target with a gas flame until the fluoride melted and flowed evenly over the surface. The effective thickness of the target is probably less than 30 kev. owing to the rapid decrease in reaction yield with decrease in energy of the triton as it penetrates the target.

The details of the target assembly are shown in Fig. 2. The target remained fixed in its position with the face at $22\frac{1}{2}°$ to the beam throughout the runs. The α-particles detected by the angular distribution counter emerged at angles varying from $63\frac{1}{2}°$ to $18\frac{1}{2}°$ with the target face depending on the position of the counter. At the smaller angles there was a noticeable broadening of the peaks due to target surface irregularities but the groups were still well defined.

RESULTS

The angular distribution of the 8.67 Mev. α-particles from the reaction $Li^7(p, \alpha)He^4$ at 240 kev. bombarding energy was observed as a test of the apparatus. In the center of mass system this distribution must be symmetric about the plane normal to the beam because the two product particles are identical. This is shown in Fig. 3 in which the points taken at angles less than

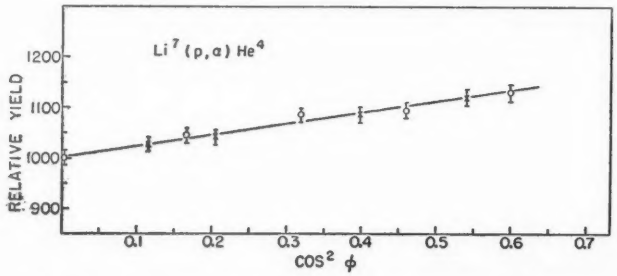

FIG. 3. The angular distribution of the $Li^7(p, \alpha)He^4$ reaction at 240 kev. proton energy. The straight line is of the form $1-0.22(\pm 0.02)\cos^2\phi$ when ϕ is the angle between the beam and the observed α-particles in the center of mass system. Points marked ○ are for $\phi < 90°$ and points × for $\phi > 90°$.

90° lie on the same line as those taken at angles greater than 90° to within $1\frac{1}{2}$% and thus provide a satisfactory check of the fore-and-aft geometry of the angular distribution chamber. Two readings were taken at each angle, one to the

left of the beam and one to the right, and the mean value used as a measure of the yield at that angle. This procedure cancelled out a small left to right asymmetry which could be accounted for by assuming that the effective center of the target was displaced 0.030 in. from the geometric center of the chamber. No attempt was made to correct this displacement since the error produced in the averaged yield at each angle was negligible.

In Fig. 4 is shown a typical pulse height distribution obtained with the angular distribution counter observing α-particles from the $Li^7(t, \alpha)He^6$

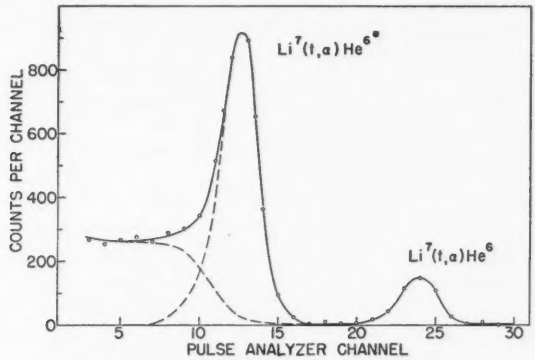

FIG. 4. A typical pulse height spectrum from the angular distribution counter taken at 90° to the beam. The discriminator bias was adjusted to allow only pulses corresponding to α-particles above about 4 Mev. to be counted on the pulse height analyzer. Thus, the two peaks under investigation are expanded over the full 30 channels and the lower part of the spectrum is cut off.

reactions. A group of large pulses due to 8.7 Mev. α-particles from the $Li^7(p, \alpha)He^4$ reaction was also present but appeared beyond the end of the distribution shown in Fig. 4 and was easily recognized. The group of large pulses due to α-particles associated with the formation of He^6 in its ground state is clearly resolved and the intensity of this group is easily ascertained at each angle. However, to measure the yield of the excited state is more difficult since the group of pulses produced by α-particles from reaction (ii) is overlapped by a continuum of pulses produced by α-particles from the four-body disintegrations $Li^7(t, 2n)2He^4$. This latter reaction may proceed either directly or as a two-step process via the formation of the unstable nuclei Be^8, He^5 and excited states of Be^9 and He^6. Hence the shape of the continuum is not known. The value of the end point can, however, be computed to be 5.3 Mev. in the center of mass system for the direct four-body breakup. For the two-step processes the value of the end point will be lower. In the present work the *relative* intensity, at different angles, of the large group at 4.9 Mev. is required. This was estimated by assuming that the right-hand side of this group was not appreciably distorted by the tail of the continuum, and the left-hand side was drawn, as indicated by the dashed curve, to make the shape the same as that of the clearly resolved higher energy group. A second analysis was made by

extrapolating the continuum by eye in a smooth curve to an end point at 5.3 Mev. This gave essentially the same angular distribution within the probable errors. Thus the criteria used to estimate the yields of reaction (ii) are necessarily somewhat arbitrary but they are believed to give the relative yields to $\pm 5\%$.

The observed data, transformed to the center of mass system, are plotted in Fig. 3 for the $Li^7(p, \alpha)He^4$ reaction at 240 kev. bombarding energy and produce an angular distribution of the form $1 + 0.22(\pm 0.02) \cos^2 \phi$. This is consistent with the earlier measurements of Young (9) which gave 0.2 for the coefficient of $\cos^2 \phi$, and also with the later data obtained by Martin *et al.* (7) using a photographic plate technique.

The results in the center of mass system for the bombardment of lithium with 240 kev. tritons are shown in Fig. 5. The reaction $Li^7(t, \alpha)He^6$, going to

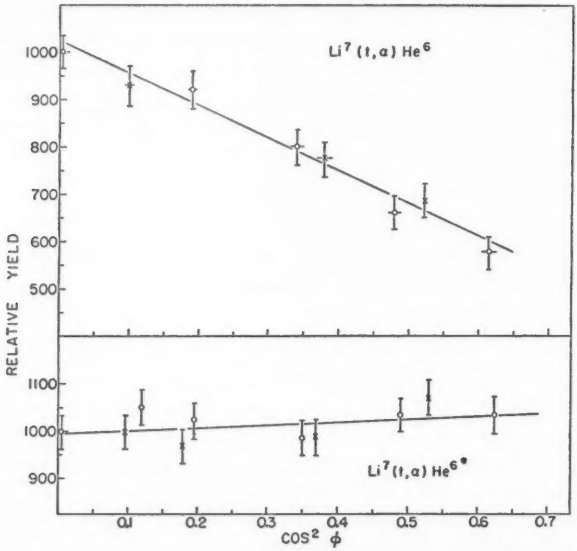

FIG. 5. The angular distribution of the $Li^7(t, \alpha)He^6$ reactions at 240 kev. triton energy. The α-particles associated with the ground state of He^6 have a distribution of the form $1-0.66(\pm 0.06) \cos^2 \phi$ when ϕ is the angle between the beam and the observed α-particles in the center of mass system. The α-particles from the reaction going to the 1.71 Mev. excited level in He^6 are distributed nearly isotropically about the beam in the center of mass system. Points marked ○ are for $\phi < 90°$ and points × for $\phi > 90°$.

the ground state of He^6, is very anisotropic with the maximum yield at 90° to the beam. Between the limits of angle of observation, the distribution is of the form $1-0.66(\pm 0.06) \cos^2 \phi$, with no evidence of any cosine term. The points observed at angles less than 90° are indicated by crosses and coincide, within the experimental errors, with those observed at angles greater than 90°, indicated by circles. Hence a cosine term, if present at all, probably has a co-

efficient less than 5% of the isotropic component. In order to obtain data about terms involving $\cos^3\phi$ or higher powers the measurements should be extended to larger values of ϕ. However, it is unlikely that such higher powers occur in the angular distribution at this low bombarding energy. Christie (4) has pointed out that the assumption of L–S coupling leads to an angular distribution of the form $1–0.79\cos^2\phi$ for this reaction which is in reasonable agreement with the observed distribution.

The angular distribution of reaction (ii) is nearly isotropic. The observed data give an angular distribution of the form

$$1 + 0.00(\pm 0.05)\cos\phi + 0.05(\pm 0.08)\cos^2\phi.$$

The angular distribution of the α-particles, in the continuum produced by the disintegrations leading to two α-particles and two neutrons, was not studied in detail, but the part of it above 4 Mev. appears roughly isotropic with some tendency for an increased yield in the fore and aft directions. If one excludes the α-particles from the decay of the excited state of He^6, it can be deduced that 80% of the disintegrations yielding α-particles are multibody, by assuming that these multibody reactions are isotropic and yield two α-particles per disintegration. The remaining 20% proceeds via the $Li^7(t, \alpha)He^6$ reactions. Of these, reaction (ii) is eight times as probable as reaction (i) at 240 kev. bombarding energy.

DISCUSSION

The anisotropic distribution of the α-particles from reaction (i) implies that this reaction is produced largely by tritons arriving with angular momentum l, greater than zero. Moreover, at 240 kev. bombarding energy, the potential barrier greatly reduces the yield due to tritons having $l \geqslant 2$. It thus seems probable that the $Li^7(t, \alpha)He^6$ reaction is produced chiefly by P-wave tritons. Additional evidence that S-wave tritons are contributing very little, if at all, to the yield of He^6 in the *ground state* is provided by the absence in the angular distribution of a cosine term which would arise from interference between incoming S and P waves. This is somewhat surprising as S-wave interactions are not, a priori, forbidden by selection rules.

On the other hand reaction (ii) has a nearly isotropic angular distribution and the total yield of He^{6*} is eight times that of He^6 from the ground state reaction. These facts, combined with the observation that reactions leading to the continuous distribution of α-particles have a yield more than 40 times that of reaction (i), suggest that the formation of ground state He^6 is restricted by selection rules that do not apply to the competing reactions.

The above observations support the expectation that the ground state of He^6, an even–even nucleus, has spin 0. In this case neither of the products of reaction (i) have intrinsic spin and the transitions are restricted to those in which the total angular momentum is converted to relative orbital motion of the α-particle and the He^6 nucleus. Such transitions to two zero-spin particles of even parity can only occur through compound states of even J, even parity, or odd J, odd parity. Thus, although S-wave tritons on Li^7 can form compound

states with odd parity and $J = 3/2 \pm 1/2$, only the state with $J = 1$ can yield He^6 with spin zero. If there exists no level in Be^{10} with $J = 1$, odd parity, near the excitation energy 17.24 Mev. produced by 240 kev. tritons on Li^7, then S-wave tritons will not contribute appreciably to reaction (i).

It is suggested that near this excitation energy in Be^{10} there is an even state with $J = 2$ which is formed by P-wave interactions. This state is the only one satisfying the above selection rule for breakup into two spinless particles of even parity that can be formed by P-wave tritons. It can also be shown by the method of Blatt and Biedenharn (3) that such a state must yield an angular distribution of the form $1 + A \cos^2 \phi$ where $3 > A > -1$, if the assignment of even parity, spin 0, is assumed for He^6. The observed distribution, $1 - 0.66 \cos^2 \phi$, of reaction (i) is therefore consistent with the reaction going through such a compound state.

The nearly isotropic angular distribution of He^{6*} may also be accounted for by this compound state. However, the absence of an S-wave contribution to reaction (i) does not exclude the possibility of S-wave tritons reacting with lithium to produce the competing reactions via a compound state with $J = 2$, *odd* parity. It is, therefore, possible that the large nearly isotropic yields of the multibody breakup and of He^{6*} are due to S-wave interactions via such a level in Be^{10}. In either case it seems likely that the level associated with the resonance in the neutron yield observed by Crews (5) at 800 kev. triton energy has $J = 2$. Further measurements at energies greater than can be attained with the 250 kv. set would show whether this level has odd or even parity.

In conclusion, therefore, the observations are qualitatively consistent with the ground state of He^6 having spin 0 and the compound nucleus being formed in a level with $J = 2$, even parity. Possibly an overlapping level with $J = 2$, odd parity, is also contributing to reaction (ii) and to the multibody breakup. It is of interest to note that the $Li^7(t, \alpha)He^6$ may proceed as a pickup reaction (inverse stripping) but at this low bombarding energy compound nucleus formation has been assumed more important.

We are indebted to Dr. W. T. Sharp of the Theoretical Physics Branch for a calculation by the method of Blatt and Biedenharn (3) of the angular distribution to be expected assuming incoming S and P wave particles, and for helpful discussions about the interpretation of the results. We also wish to thank Mr. J. W. Jagger whose technical assistance was invaluable in maintaining and operating the 250 kv. set, and Dr. L. G. Elliott for encouraging interest throughout the work.

REFERENCES

1. Allen, K. W., Almqvist, E., Dewan, J. T., and Pepper, T. P. Can. J. Phys. 29: 557. 1951.
2. Allen, K. W., Almqvist, E., Dewan, J. T., Pepper, T. P., and Sanders, J. H. Phys. Rev. 82: 262. 1951.
3. Blatt, J. M. and Biedenharn, L. C. Revs. Mod. Phys. 24: 258. 1952.
4. Christie, R. F. Phys. Rev. 89: 839. 1953.
5. Crews, R. W. Phys. Rev. 82: 100. 1951.

6. DEWAN, J. T., PEPPER, T. P., ALLEN, K. W., and ALMQVIST, E. Phys. Rev. 86: 416. 1952.
7. MARTIN, L. H., BOWER, J. C., DUNBAR, D. N. F., and HIRST, F. Australian J. Sci. Research, Ser. A, 2: 25. 1949.
8. PEPPER, T. P., ALLEN, K. W., ALMQVIST, E., and DEWAN, J. T. Phys. Rev. 81: 315A. 1951; 85: 155. 1952.
9. YOUNG, V. J., ELLET, A., and PLAIN, G. J. Phys. Rev. 58: 498. 1940.

HIGH RESOLUTION RAMAN SPECTROSCOPY OF GASES

III. RAMAN SPECTRUM OF NITROGEN[1]

By B. P. Stoicheff

ABSTRACT

The pure rotational spectrum and the Q branch of the 1–0 band of N_2 were photographed in the second order of a 21 ft. grating. An analysis of the rotational spectrum yields the rotational constants

$B_0 = 1.9897_3 \pm 0.0003$ cm.$^{-1}$ and $D_0 = (6.1 \pm 0.5) \times 10^{-6}$ cm^{-1}.

The value of B_0 together with the B_v values obtained from the electronic bands of N_2 gives

$$B_e = 1.9987_4 \pm 0.0003_5 \text{ cm}^{-1}.$$

Hence $r_e = 1.0975_8 \pm 0.0001$ Å.

Revised values of the vibrational constants have also been calculated using the results of the present work and the published data on the electronic spectra.

A. INTRODUCTION

One of the first rotational Raman spectra to be photographed was that of the nitrogen molecule. This spectrum was obtained by Rasetti (8) in 1929. Recently the rotational Raman spectrum of nitrogen was photographed with a 21 ft. grating spectrograph under considerably higher resolution than the earlier work. It seemed worth while to analyze the spectrum and to compare the values of the rotational constants thus obtained with the existing values.

The molecular constants of N_2 have been tabulated by Herzberg (5). For the ground electronic state, the vibrational constants were obtained by Birge and Hopfield (2) from bands of the Lyman–Birge–Hopfield system, and the rotational constants were evaluated by Setlow (9) from the combined data of the Raman spectrum and the extensive electronic spectra of nitrogen. The value of the rotational constant B_0 found in the present research is significantly different from the value given by Setlow and yields a somewhat higher value for the internuclear distance in the nitrogen molecule.

B. OBSERVED SPECTRUM

The apparatus was described in paper I of this series (11). Three photographs of the nitrogen rotational spectrum were obtained in the second order of the 21 ft. grating on Kodak 103 a-0 plates. Up to 35 lines were photographed in exposure times of 12 to 24 hr. with the gas at a pressure of 2 atm. One of these photographs is shown in Fig. 1. The spectrum consists of a series of widely-spaced lines showing the characteristic alternation of intensity: strong, weak, strong, weak. . . . The rotational lines are quite sharp even at this relatively high gas pressure. Although there are many grating ghosts, they are widely spaced and only interfere with the measurement of the two lines closest to the exciting line.

The plates were evaluated as in paper II (12). The wave number shifts

[1]*Manuscript received June 28, 1954.*
Contribution from the Division of Physics, National Research Laboratories, Ottawa, Canada. Issued as N.R.C. No. 3367.

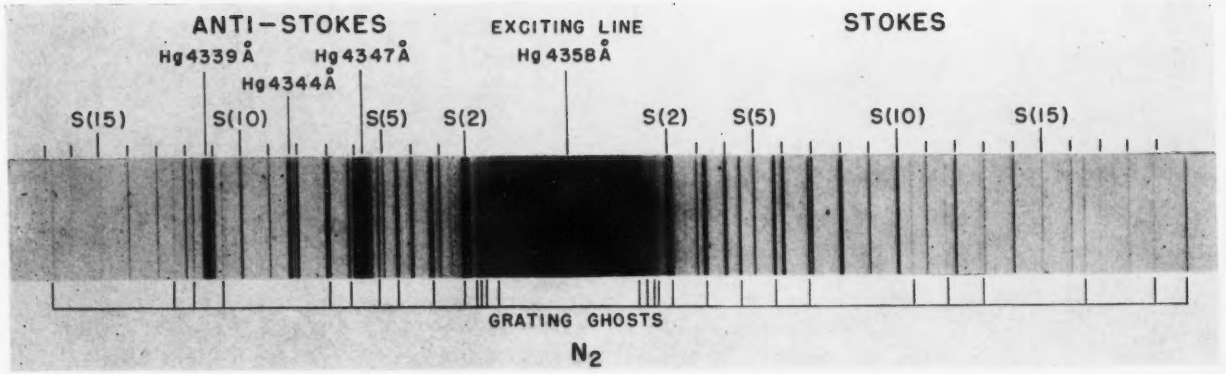

FIG. 1. Rotational Raman spectrum of N_2 photographed in the second order of a 21 ft. grating.

measured from the three plates were averaged and these values are given in Table I. From a comparison of the wave number shifts obtained from the

TABLE I

OBSERVED AND CALCULATED WAVE NUMBER SHIFTS OF THE ROTATIONAL RAMAN LINES OF N_2

J	$\lvert\Delta\nu\rvert^{a}_{obs}$(cm.$^{-1}$)	$\lvert\Delta\nu\rvert_{calc}$(cm.$^{-1}$)	Obs−Calc (cm.$^{-1}$)
0	—	11.938	—
1	19.908[b]*	19.896	+0.012
2	27.857*	27.854	+0.003
3	35.812	35.811	+0.001
4	43.762	43.766	−0.004
5	51.721	51.719	+0.002
6	59.662	59.671	−0.009
7	67.629	67.621	+0.008
8	75.566*	75.568	−0.002
9	83.504	83.512	−0.008
10	91.455	91.453	+0.002
11	99.406*	99.391	+0.015
12	107.327	107.325	+0.002
13	115.243	115.255	−0.012
14	123.189	123.181	+0.008
15	131.093	131.102	−0.009
16	139.024	139.019	+0.005
17	146.901[b]	146.930	−0.029
18	154.849	154.836	+0.013
19	162.752[b]	162.737	+0.015

[a] *All values are averages of the Stokes and anti-Stokes lines measured on three plates, except the values marked* [b].

[b] *Stokes lines measured on one plate only.*

* *Indicates lines blended with grating ghosts.*

different plates, it is estimated that lines of medium or higher intensity have been measured to an accuracy of ± 0.03 cm^{-1}.

The Q branch of the 1–0 band also appeared on the plates. It is a faint broad band degraded to the violet forming a band head at a displacement of 2329.66 cm.$^{-1}$ from the exciting line.

C. ROTATIONAL ANALYSIS

For a diatomic molecule, the wave number shifts (units cm.$^{-1}$) of the pure rotational Raman lines are given by the equation

[1] $$|\Delta\nu| = (4B_0 - 6D_0)(J+\tfrac{3}{2}) - 8D_0(J+\tfrac{3}{2})^3$$

where

$$B_0 = (27.989_{03}/I_0)\times 10^{-40} \text{ cm}^{-1}.*$$

For a vibrating diatomic molecule, the rotational constant B_0 is replaced by B_v where

[2] $$B_v = B_e - \alpha_e(v+\tfrac{1}{2}) + \ldots$$

in the standard notation (5).

* *The 1952 atomic constants given by DuMond and Cohen (3) were used in this calculation.*

The analysis of the observed rotational spectrum was based on equation [1]. The rotational numbering was readily determined since the rotational lines nearest to the exciting line could be identified. A graph of $|\Delta\nu|/(J+\frac{3}{2})$ vs. $(J+\frac{3}{2})^2$ was then plotted, as shown in Fig. 2. The experimental points lie on a

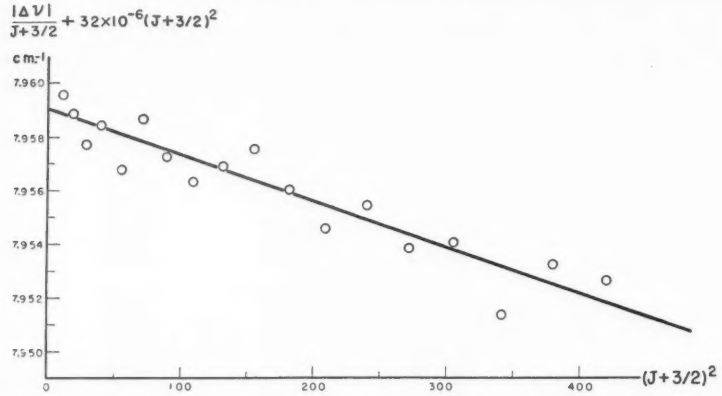

FIG. 2. $|\Delta\nu|/(J+3/2)$ for the ground state of N_2. The term $32\times10^{-6}(J+3/2)^2$ has been added to $|\Delta\nu|/(J+3/2)$ in order to allow a large-scale plot.

straight line whose intercept on the ordinate axis gives $4B_0-6D_0$ and whose slope gives $8D_0$. The values obtained from this graph are

$$B_0 = 1.9897_3\pm0.0003 \text{ cm.}^{-1}, \qquad D_0 = (6.1\pm0.5)\times10^{-6} \text{ cm}^{-1}.$$

Therefore $I_0 = (14.067_0\pm0.002)\times10^{-40}$ gm. cm.^{2},

and $r_0 = 1.1000_6\pm0.0001$ Å.

The experimental value of D_0 compares favorably with the value 5.8×10^{-6} cm.$^{-1}$ calculated from the theoretical relation $D_e = 4B_e^3/\omega_e^2$. The wave number shifts of the N_2 rotational lines were calculated using the rotational constants obtained here, and these are shown in Table I for comparison with the measured values. In almost every case, the agreement is within ±0.02 cm^{-1}.

D. DISCUSSION

The value of the rotational constant B_0 is in good agreement with Rasetti's value $B_0 = 1.992\pm0.005$ cm.$^{-1}$, but differs markedly from Miller's value $B_0 = 1.980$ cm.$^{-1}$ (7).* The most recent evaluation of B_0 was made by Setlow (9). His value $B_0 = 2.0007\pm0.0027$ cm.$^{-1}$ is considerably higher than that found here. Setlow's value was obtained from a least squares calculation using Rasetti's value and the data of Spinks (10), Appleyard (1), Watson and Koontz (14), and Tschulanowsky (13) on the electronic bands of N_2. This determination is based mainly on a linear extrapolation of B_v values from

*There appears to be an error in Miller's interpretation; when this is corrected, his data yield $B_0 = 1.988$ cm^{-1}.

$v = 10$ to 21 and may be in error owing to this long extrapolation. Moreover, the accuracy of the B_v values determined from the electronic bands is lower than might be desired since the requisite resolution was not available for these investigations.

In order to calculate the constant B_e, and hence the equilibrium internuclear distance, α_e must be known. According to equation [2], α_e can be found from a graph of B_v vs. $(v+\frac{1}{2})$. At present, an accurate value of this constant is not available since a sufficient number of B_v's have not been evaluated. Nevertheless, an approximate value for α_e can be obtained from the available electronic data and the B_0 value determined here. A B_v graph is shown in Fig. 3. In drawing this graph, a linear relation was assumed and a straight

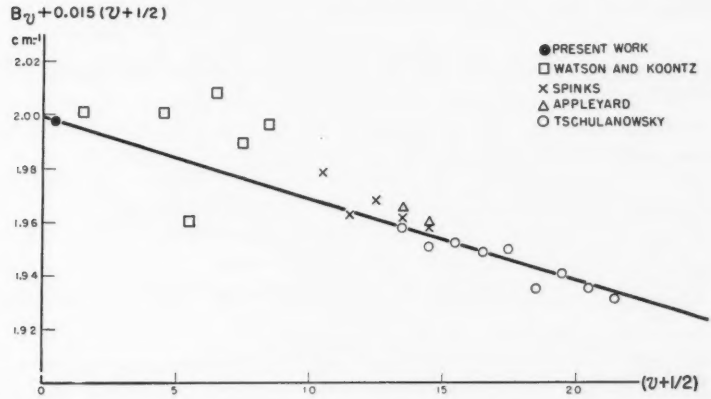

FIG. 3. B_v graph for the ground electronic state of N_2. The value $0.015(v+\frac{1}{2})$ has been added to B_v in order to allow a large-scale plot.

line was drawn through the point representing the present Raman value of B_0. The straight line which appears to give the "best" fit has a slope of 0.01803 ± 0.0001 cm^{-1}. This value of α_e is chosen here. Perhaps higher order terms in $(v+\frac{1}{2})$ should be included in equation [2], but it is difficult to assess the accuracy of the available data and it appears that a linear relation may be sufficiently good.

This analysis of the spectroscopic data available at present yields the following values:

$$B_e = 1.9987_4\pm0.0003_5 \text{ cm.}^{-1},$$
$$I_e = (14.003_5\pm0.002_6)\times10^{-40} \text{ gm. cm.}^2,$$
$$r_e = 1.0975_8\pm0.0001 \text{ Å}.$$

When the vibrational constants of Birge and Hopfield are used to calculate the wave number shift of the 1–0 band, a value 1 cm.$^{-1}$ higher than that measured here (section B) is obtained. Although the Raman value of 2329.66 cm.$^{-1}$ is based on the measurement of the band head formed by the Q branch,

it probably gives the position of the band center to within ± 0.2 cm.$^{-1}$; that is $\Delta G_{\frac{1}{2}} = 2329.66 \pm 0.2$ cm^{-1}. The discrepancy of 1 cm.$^{-1}$ is considerably larger than the error of measurement and suggests that the vibrational constants need revision. A redetermination of these constants has been made using the Raman value for $\Delta G_{\frac{1}{2}}$ and the electronic data of Birge and Hopfield (2), Spinks (10), Tschulanowsky (13), Setlow (9), Herman (4), and Janin (6) for vibrational levels up to $v = 20$. The coefficients of a third-order equation for the term values $G(v)$ are:

$$\omega_e = 2357.84 \text{ cm.}^{-1}; \qquad \omega_e x_e = 14.062 \text{ cm.}^{-1}; \qquad \omega_e y_e = -0.0175 \text{ cm}^{-1}.$$

Clearly, in order to obtain more accurate values of the rotational and vibrational constants of N_2, further data from the electronic bands in the ultraviolet are desirable.

I wish to thank Dr. G. Herzberg and Dr. A. E. Douglas for helpful discussions.

REFERENCES

1. Appleyard, E. T. S. Phys. Rev. 41: 254. 1934.
2. Birge, R. T. and Hopfield, J. J. Astrophys. J. 68: 257. 1928.
3. DuMond, J. M. W. and Cohen, E. R. Revs. Mod. Phys. 25: 691. 1953.
4. Herman, R. Ann. phys. 20 (11): 241. 1945; Nature, 157: 843. 1946.
5. Herzberg, G. Spectra of diatomic molecules. D. Van Nostrand Company, Inc., New York. 1950.
6. Janin, J. Ann. phys. 1 (12): 538. 1946.
7. Miller, C. E. J. Chem. Phys. 6: 902. 1938.
8. Rasetti, F. Nature, 123: 759. 1929; Z. Physik, 61: 598. 1930; Phys. Rev. 34: 367. 1929.
9. Setlow, R. B. Phys. Rev. 74: 153. 1948.
10. Spinks, J. W. T. Can. J. Research, A, 20: 1. 1942.
11. Stoicheff, B. P. Can. J. Phys. 32: 330. 1954.
12. Stoicheff, B. P. Can. J. Phys. 32: 339. 1954.
13. Tschulanowsky, W. M. Bull. acad. sci. U.R.S.S. 1: 1313. 1935.
14. Watson, W. W. and Koontz, P. G. Phys. Rev. 46: 32. 1934.

HIGH RESOLUTION RAMAN SPECTROSCOPY OF GASES

IV. ROTATIONAL RAMAN SPECTRUM OF CYANOGEN[1]

By C. K. Møller[2] and B. P. Stoicheff

ABSTRACT

The rotational Raman spectrum of cyanogen gas at ½ atm. pressure has been photographed in the second order of a 21 ft. concave grating spectrograph. The simplicity of the spectrum and the observed intensity alternation of the lines show that C_2N_2 is a linear symmetric molecule. An analysis of the spectrum yields for the rotational constants

$$B_0 = 0.15752 \pm 0.00015 \text{ cm.}^{-1} \text{ and } D_0 = 4 \times 10^{-8} \text{ cm}^{-1}.$$

By assuming a value for the C≡N bond length of 1.157 Å, the length of the C—C single bond was calculated to be 1.380 Å.

A. INTRODUCTION

In principle, the rotational constants B_0 and D_0 for the ground state of a linear molecule are easily obtained from the rotational structure of the infrared vibration bands (3); in practice, however, difficulties are often encountered due to overlapping bands. Such is the case with cyanogen for which Craine and Thompson (1) have recently analyzed the rotational structure of the ν_3 band. Because of overlapping "hot" bands, they were not able to locate the band center with certainty and it is now found that their numbering of the rotational lines is incorrect. In the rotational Raman spectrum, on the other hand, an unambiguous numbering can be obtained.

B. EXPERIMENTAL

Cyanogen was prepared by slowly adding a concentrated solution of potassium cyanide to a concentrated solution of copper sulphate. The gas was purified by distillation in vacuum and dried over phosphorus pentoxide.

The Raman apparatus has been described previously in paper I of this series (8). As in this earlier work, the Raman spectrum was photographed in the second order of a 21 ft. grating. For the initial plates, a pressure of 1 atm. of C_2N_2 was used, but as it was found that the rotational lines were considerably pressure broadened, ½ atm. was used for subsequent plates. In this way two plates with sharp lines were obtained in exposure times of 15 and 20 hr. Fig. 2 shows a reproduction of the spectrum. The plates were evaluated by the method described previously (9).

C. ANALYSIS

For a linear molecule like C_2N_2, the rotational energy levels of the ground state are given by the equation (3):

$$F(J) = B_0 J(J+1) - D_0 J^2(J+1)^2$$

and the selection rule for the rotational Raman spectrum is $\Delta J = 0, \pm 2$.

[1]*Manuscript received June 28, 1954.*
Contribution from the Division of Physics, National Research Council, Ottawa, Canada. Issued as N.R.C. No. 3368.
[2]*National Research Laboratories Postdoctorate Fellow.*

Hence, the frequency shifts, $\Delta\nu$, of the Raman rotational lines relative to the exciting line are given by

$$|\Delta\nu| = (4B_0 - 6D_0)(J+\tfrac{3}{2}) - 8D_0(J+\tfrac{3}{2})^3.$$

The numbering of the rotational lines is obtained by dividing the frequency shifts by the average frequency difference between successive Raman lines ($\approx 4B_0$). Thus, the correct J numbering having been obtained, the average of the frequency shifts of the Stokes and anti-Stokes lines with the same J was divided by $J+\frac{3}{2}$ and plotted against $(J+\frac{3}{2})^2$, as shown in Fig. 1. This

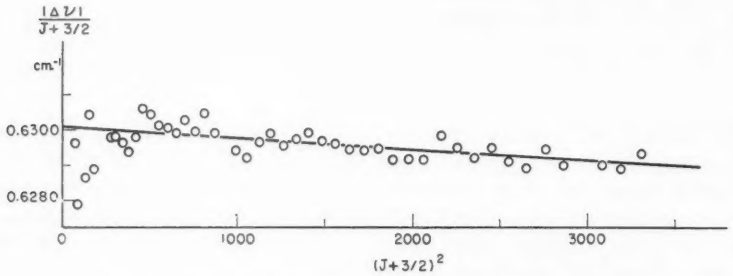

FIG. 1. $|\Delta\nu|/(J+3/2)$ graph for the ground state of C_2N_2.

gave a straight line having an intercept on the ordinate axis of $4B_0-6D_0$ and a slope of $8D_0$. The mean values of the rotational constants from two plates are:

$$B_0 = 0.15752 \pm 0.00015 \text{ cm.}^{-1}, \qquad D_0 = (4\pm 2)10^{-8} \text{ cm}^{-1}.$$

Calculation of D_0 from force constants and internuclear distances in C_2N_2 using a general force field (6) yields 1.3×10^{-8} cm.$^{-1}$ and using a valence force field (3), about 2.5×10^{-8} cm^{-1}. The lack of agreement between the observed and experimental values is not understood at present, but may possibly indicate a small systematic error in the present Raman work. For this reason, rather liberal errors have been given for the values of the rotational constants. Table I gives the observed frequency shifts and also, for comparison, the frequency shifts calculated from $B_0 = 0.15752$ cm.$^{-1}$ and $D_0 = 4.0\times10^{-8}$cm^{-1}.

The observed rotational Raman spectrum of C_2N_2 is produced partly by molecules in the ground state and partly by molecules in the first excited vibrational level at 230 cm^{-1}. The contribution from molecules in the higher excited levels is much less and can be neglected for the present purposes. The first excited vibrational level is doubly degenerate and has a Boltzmann factor of about two-fifths. Hence, the pure rotational spectrum produced by molecules in this level would be expected to have about four-fifths of the intensity of the spectrum due to molecules in the ground state. These spectra may not coincide exactly owing to small differences in the values of the rotational constants of the two vibrational levels. The observed lines would then be slightly shifted from the positions corresponding to the ground state

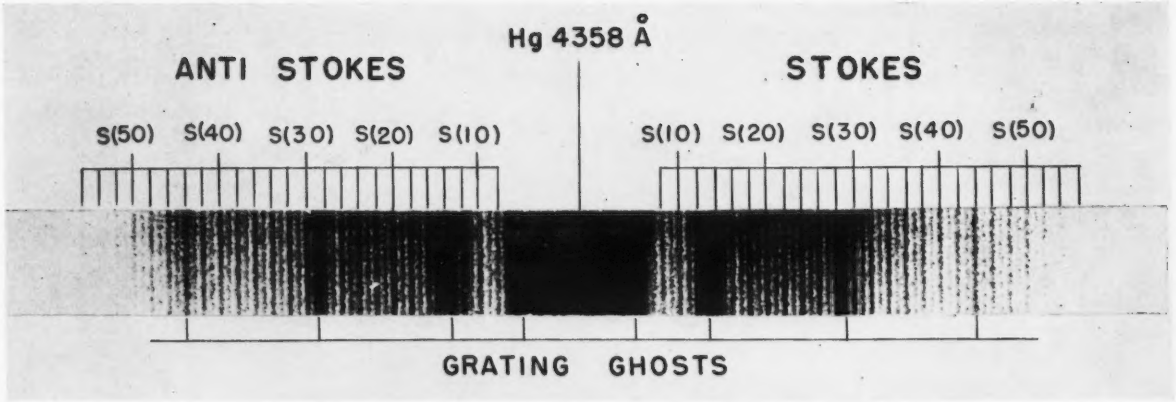

FIG. 2. Rotational Raman spectrum of C_2N_2 photographed in the second order of a 21 ft. grating.

TABLE I

OBSERVED AND CALCULATED FREQUENCY SHIFTS $|\Delta\nu_{vac}|$ IN CM.$^{-1}$ FOR THE ROTATIONAL RAMAN SPECTRUM OF C_2N_2

J	Observed** $\lvert\Delta\nu\rvert$	Calculated $\lvert\Delta\nu\rvert$	Obs − Calc	J	Observed** $\lvert\Delta\nu\rvert$	Calculated $\lvert\Delta\nu\rvert$	Obs − Calc
7	5.36_7	5.35_6	0.01_1	31	20.44_9	20.46_7	-0.01_8
8	5.96_5	5.98_6	-0.02_1	32	21.09_3	21.09_6	-0.00_3
9	6.57_3	6.61_5	-0.04_2	33	21.73_0	21.72_5	0.00_5
10	7.23_0	7.24_5	-0.01_5	34	22.34_9	22.35_4	-0.00_5
				35	22.98_5	22.98_2	0.00_3
11	7.88_0	7.87_5	0.00_5	36	23.62_1	23.61_1	0.01_0
12	8.49_0	8.50_6	-0.01_6	37	24.24_3	24.24_0	0.00_2
13*	—	9.13_6	—	38	24.86_8	24.86_8	0.00_0
14*	—	9.76_4	—	39	25.49_4	25.49_7	-0.00_3
15	10.39_2	10.39_4	-0.00_2	40	26.11_9	26.12_6	-0.00_7
16	11.02_2	11.02_5	-0.00_3				
17	11.64_8	11.65_5	-0.00_7	41	26.75_0	26.75_3	-0.00_3
18*	12.27_3	12.28_4	-0.01_1	42	27.36_7	27.38_2	-0.01_5
19	12.91_0	12.91_4	-0.00_4	43	27.99_7	28.01_1	-0.01_4
20*	13.55_8	13.54_4	0.01_4	44*	28.62_5	28.63_8	-0.01_3
				45	29.28_6	29.26_7	0.01_9
21	14.17_4	14.17_3	0.00_1	46	29.90_1	29.89_5	0.00_6
22	14.80_8	14.80_3	0.00_5	47	30.51_6	30.52_2	-0.00_6
23	15.43_6	15.43_2	0.00_4	48	31.15_7	31.15_0	0.00_7
24	16.06_3	16.06_1	0.00_2	49	31.76_9	31.77_8	-0.00_9
25	16.70_2	16.69_1	0.01_1	50	32.38_8	32.40_5	-0.01_7
26	17.32_4	17.32_1	0.00_3				
27	17.96_9	17.95_0	0.01_9	51	33.04_7	33.03_3	0.01_4
28*	18.58_2	18.57_9	0.00_3	52	33.64_9	33.66_1	-0.01_2
29*	—	19.20_8	—	53	34.26_9	34.28_7	-0.01_8
30	19.82_5	19.83_7	-0.01_2	54	34.90_7	34.91_4	-0.00_7
				55	35.53_1	35.54_2	-0.01_1
				56	36.18_3	36.16_9	0.01_4

**Blended with grating ghosts.*

***Average values of frequency shifts of corresponding Stokes and anti-Stokes lines from two plates.*

rotational spectrum and would yield a B value which is an average for the two levels rather than a value of B_0. However, the difference between the B value of the ground state and that of the lowest-lying degenerate level is usually very small for linear molecules, e.g., for CO_2, it is about 0.15% of the B_0 value (3). It therefore seems unlikely that the B value obtained here differs appreciably from the value of B_0.

D. DISCUSSION

The pronounced intensity alternation and the very simple structure of the rotational Raman spectrum show that C_2N_2 is a linear symmetric molecule. A very different spectrum would result if C_2N_2 were non-linear. If it were bent by a large amount and an asymmetric top, a very complicated spectrum would result because of the complex energy levels and selection rules. For small deviations from the linear structure, the molecule would be approximately a prolate symmetric top. It would have a relatively simple spectrum similar to that of a linear molecule except that now each line will be a superposition of lines corresponding to the different K values. Only the line components with $K = 0$ will show an intensity alternation (see Fig. 8(a) of Ref. (3)), and since the levels with $K \neq 0$ would undoubtedly be populated, there would be

practically no evidence of intensity alternation, contrary to the observed spectrum of C_2N_2. The pronounced intensity alternation clearly excludes a bent structure for the C_2N_2 molecule.

The moment of inertia calculated from the value $B_0 = 0.1575_2$ cm.$^{-1}$ and the atomic constants of DuMond and Cohen (2) is $I_0 = 177.6_9 \times 10^{-40}$ gm. cm.^{2} A determination of the C—C single bond distance may then be made from the moment of inertia if the length of the C≡N bond is assumed. The value chosen here is r_0(C≡N) = 1.157 Å as found by Westenberg and Wilson (10) from the microwave spectrum of cyanoacetylene. This leads to the length r_0(C—C) = 1.380 Å. This value is in agreement with the electron diffraction values of 1.37±0.02 Å (7) and 1.38±0.02 Å (6) within the limits of measurement of the latter method. It is interesting to note that the C—C bond length in cyanogen is considerably shorter than the normal single bond of 1.54 Å. This result is in agreement with the short C—C single bonds found by Herzberg, Patat, and Verleger (4) and Jones (5) in methylacetylene and diacetylene where, as in cyanogen, the single bond is adjacent to triple bonds.

Craine and Thompson (1) obtained somewhat higher values for the rotational constants of C_2N_2: $B_0 = 0.1588 \pm 0.0001$ cm.$^{-1}$, $D_0 = 11 \times 10^{-8}$ cm^{-1}. Their resulting value of r_0(C—C) is therefore slightly lower than the value calculated above. However, Craine and Thompson mention the possibility of shifting their J numbering by two units. If this is done, the revised value for B_0 is in substantial agreement with that found here, which is based on an unambiguous numbering. They consider their D_0 value only as an upper limit.

In order to make a spectroscopic determination of the two internuclear distances in C_2N_2 free from any assumptions about the C≡N bond length, it will be necessary to carry out a similar investigation with one of the isotopes of cyanogen, for example, $N^{15}C^{12}C^{12}N^{14}$. However, a pure sample would be necessary since the present resolution, limited by pressure broadening of the Raman lines and the width of the exciting line, would not be sufficient to separate the lines of the Raman spectrum of a mixture of isotopic cyanogen molecules.

It is a pleasure to acknowledge our indebtedness to Dr. A. E. Douglas and to Dr. G. Herzberg for helpful discussions.

REFERENCES

1. Craine, G. D. and Thompson, H. W. Trans. Faraday Soc. 49: 1273. 1953.
2. DuMond, J. M. W. and Cohen, E. R. Revs. Mod. Phys. 25: 691. 1953.
3. Herzberg, G. Infrared and Raman spectra. D. Van Nostrand Company, Inc., New York. 1945.
4. Herzberg, G., Patat, F., and Verleger, H. J. Phys. Chem. 41: 123. 1937.
5. Jones, A. V. J. Chem. Phys. 20: 860. 1952.
6. Langseth, A. and Møller, C. K. Acta Chem. Scand. 4: 725. 1950.
7. Pauling, L., Springall, H., and Palmer, K. J. J. Am. Chem. Soc. 61: 927. 1939.
8. Stoicheff, B. P. Can. J. Phys. 32: 330. 1954.
9. Stoicheff, B. P. Can. J. Phys. 32: 339. 1954.
10. Westenberg, A. A. and Wilson, E. B. J. Am. Chem. Soc. 72: 109. 1950.

THE AMERICAN WIND TURBINE[1]

By R. H. Nilberg

ABSTRACT

The windmill theory published by Prof. A. Betz of Göttingen does not take into account the rotational motion of the air stream behind the mill, which is quite large behind the low-speed multiblade "American wind turbine". This paper presents a theory of the low-speed wind turbine showing that the shape of the airfoil blade is predetermined by the theoretical deflection of the air stream and should not be chosen arbitrarily. An increase of starting torque and efficiency of about twenty per cent may be expected.

INTRODUCTION

Despite vast motorization of farms, the American wind turbine is still very popular, especially on prairie farms and ranches where it is used mostly for the pumping of water. It is to be found on farms throughout the world; in countries like Argentina, which have to import their motor fuel, pumping of water by means of windmills is of vital importance.

The disk of the American low-speed wind turbine is densely covered with airfoil blades manufactured from sheet iron, is of 8 to 12 ft. in diameter, and is mounted with its gear box on a 50 to 75 ft. tower. The American wind turbine has a good starting torque so that it will start under the load of a water pump. This high starting torque at low wind speeds is the main reason for its popularity. Further, a wind turbine is cheaper to operate than a motor pump, despite the generally higher price for the unit and mounting.

The theory of the "ideal windmill" was established by Prof. A. Betz of the university of Göttingen. In his study, published in 1927, he showed that an "ideal windmill" could extract only 16/27 of the power in the wind. It is supposed to have no frictional drag losses between wind stream and airfoil blade, no deflection of the wind by the airfoil, no turbulence due to incorrect shape of the airfoil.

A high-speed windmill with a tip speed of eight times the wind velocity has only two or three blades and corresponds closely to the "ideal mill". The deflection of the wind by the airfoil blades is negligible and if the airfoil blades are constructed in accordance with the latest achievements on high-speed propeller blades, losses due to friction and turbulence are very small and scarcely affect the efficiency. The high-speed windmill has a very good efficiency (about 80% of the "ideal mill"), but a very bad starting torque. It requires unloaded starting and smooth loading, and is therefore generally used only for generation of electricity. Although a dynamo always starts at no load, a special automatic starting coupling is necessary to disconnect the blade hub from the gearing of the dynamo.

The American wind turbine has a tip speed equal to the acting wind velocity. The speed of the blade element near the hub is only one quarter or less of the acting wind speed. In order to produce the same work as a high-speed mill of

[1]*Manuscript received June 7, 1954.*
Contribution from the Department of Physics, B.C. Research Council, Vancouver, B.C.

the same diameter, the low-speed mill must have roughly eight times higher torque. Higher forces on the blades can be obtained only by a relatively sharp deflection of the wind stream by the blades, and a multitude of blades is necessary to produce that deflection.

The deflection of the air stream by the blades of a low-speed mill is the reason for the rotational motion of the whole air stream behind the mill. A considerable amount of energy is lost for the low-speed mill owing to this rotational motion. The efficiency of a good low-speed wind turbine is about 45% of the "ideal mill".

Improvement of starting torque and efficiency are possible if losses due to rotation of the air stream are taken into account by the theory. The theoretical efficiency of the American wind turbine is near 75% of the "ideal mill', so that increase of torque and efficiency up to 20% may be expected.

The shape of the airfoil blade must be such that the air stream through the mill disk is deflected in the theoretically required manner. The lengthwise broken blade *A-B-C* as shown by Fig. 3 and Fig. 6 is the new shape of the airfoil. Section 5 of the "Discussion" gives an example for the design of the blade.

GENERAL THEORY

Nomenclature

v_1—Axial wind velocity far before the disk of the mill (m./sec.).

v_r'—Axial wind velocity in the disk of the mill, at the distance r from the axis (m./sec.).

v_r—Axial wind velocity far behind the disk of the mill (m./sec.).

u_r—Speed of the disk (m./sec.).

o_r—Rotational velocity of the wind behind the mill disk (m./sec.).

R—Radius of the mill disk (m.).

r—Radius of a circle in the mill disk (m.).

F_1—Sectional area of the acting wind stream far before the disk (m.^{2}).

F'—Area of the mill disk (m.^{2}).

F_2—Sectional area of the acting wind stream far behind the disk (m.^{2}).

p_0—Absolute pressure far before and far behind the disk (kgm./m.^{2}).

p'—Absolute pressure directly before the disk (kgm./m.^{2} = mm. water column).

p''—Absolute pressure directly behind the disk (kgm./m.^{2}).

γ—Mass density of air (kgm./m.^{3}); $\gamma = 1.3$ kgm./m.^{3}

g—Gravitational acceleration (m./sec.^{2}); $g = 9.81$ m./sec.^{2}; $\rho = \gamma/g = 0.13$.

U_r—Wind velocity in front of the disk relative to the moving blade (m./sec.).

W_r'—Wind velocity directly behind the disk relative to the moving blade (m./sec.).

w_r'—Absolute wind velocity directly behind the disk (m./sec.).

w_r—Absolute wind velocity far behind the disk (m./sec.).

f—Sectional ring areas of an elementary air cone, as f_1, f_r', f_r (m.^{2}).

e_r—Useful wind energy through the elementary ring area f_r' of the disk (kgm-m./sec.).

k_x—Torque force of the elementary ring area f_r' (kgm.).
k_y—Thrust of the elementary ring area f_r' in direction of axis (kgm.).
$\mathbf{k} = \mathbf{k}_x + \mathbf{k}_y$.
$K_{x,y}$—Corresponding torque force and thrust for the whole disk (kgm.).
τ—Pressure loss due to friction and turbulence (kgm./m.^{2}).
E—Total useful energy in the disk (kgm-m./sec.).
n—Ratio of blade tip speed to wind velocity $-u_R/v_1$. Further: $m_r = n(r/R)$.

Note: Index r refers either directly to the disk, at distance r from the axis, or in case of o_r, w_r, v_r, f_r it refers to air particles that have passed the disk at the distance r.

A narrow ring of the mill disk at the radius r and height Δr, as shown by Fig. 1, is analyzed. In accordance with the nomenclature it is possible to

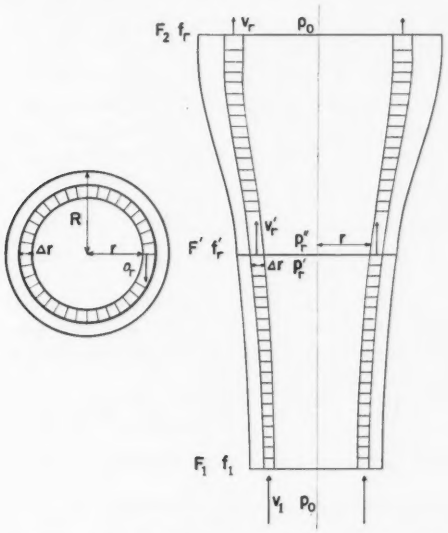

FIG. 1. Elementary air cone of the wind stream passing the disk.

write

$$f_r' = 2\pi r \cdot \Delta r \text{ and } F' = \sum f_r'.$$

The continuity of the air flow can be written as follows:

[1] $$v_1 f_1 = v_r' f_r' = v_r f_r.$$

The deflection of the air stream behind the mill, represented by vector o_r, has no influence on equation [1], because it is parallel to planes f_r' and f_r.

The air particles behind the mill are forced into a rotational motion around the axis of the disk, at the speed o_r. Free motion due to the initial vector $\mathbf{o}_r$ would tend to leave a vacuum around the axis; this is opposed by the air pressure. The rotational velocity o_r is low near the tip of the blade and high

near the hub and constant along the periphery of the radius r. The angular velocity of this rotational motion is low at the blade tips and high near the hub. The angular velocity changes considerably along the radius and the rotational motion is therefore converted in turbulence, so that velocity o_r in section F_2 has a mere theoretical value; it represents a certain amount of turbulent energy.

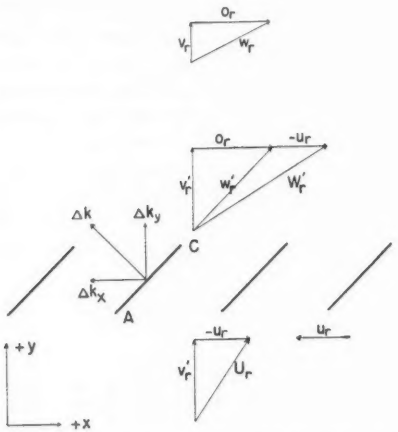

FIG. 2. Velocity vectors before and behind the disk.

A short part of the elementary disk ring is shown in Fig. 2. The following equations hold for the velocity vectors:

$$\mathbf{U}_r = \mathbf{v}_r' - \mathbf{u}_r, \qquad \mathbf{W}_r' = \mathbf{v}_r' + \mathbf{o}_r - \mathbf{u}_r,$$

[2]

$$\mathbf{w}_r' = \mathbf{v}_r' + \mathbf{o}_r, \qquad \mathbf{w}_r = \mathbf{v}_r + \mathbf{o}_r.$$

Bernoulli showed that in any mass flow the loss of kinetic energy is converted into potential energy and appears as a rise in pressure, always ready to be converted into kinetic energy again. According to Bernoulli, his formula for the acting air stream before the disk may be written in technical units as follows:

$$f_1\, v_1(\rho/2 \cdot v_1^2 + p_0) = f_r' v_r' [\rho/2 \cdot (v_r')^2 + p_r'].$$

Taking into account formula [1] it is possible to write:

[3] $$\rho/2 \cdot v_1^2 + p_0 = \rho/2 \cdot (v_r')^2 + p_r'.$$

Behind the disk, the following equations hold:

$$p_r'' + \rho/2 \cdot (w_r')^2 = p_0 + \rho/2 \cdot (w_r)^2;$$

[4] $$(w_r')^2 = (v_r')^2 + (o_r)^2, \quad (w_r)^2 = v_r^2 + o_r^2;$$

$$\rho/2 \cdot (v_r')^2 + p_r'' = \rho/2 \cdot v_r^2 + p_0.$$

No direct use of Bernoulli's formula can be made for the flow before and behind the mill disk, because the wind gives a part of its energy to the disk. With respect to the moving blade, Bernoulli's formula may be used for the relative velocities before and behind the mill disk. A supposed observer on the blade will measure the static pressures p_r' and p_r'' as if from the ground.

The relative wind velocity in front of the disk is:

$$\mathbf{U}_r = \mathbf{v}_r' - \mathbf{u}_r, \qquad U_r^2 = (v_r')^2 + (u_r)^2.$$

The relative wind velocity behind the disk is:

$$\mathbf{W}_r' = \mathbf{v}_r' + \mathbf{o}_r - \mathbf{u}_r, \qquad (W_r')^2 = (v_r')^2 + (o_r - u_r)^2.$$

Bernoulli's formula gives the following relation for these relative velocities:

[5] $$p_r' - p_r'' = \rho/2 \cdot o_r(o_r - 2u_r) + \tau.$$

Losses due to friction and turbulence are represented as pressure loss τ.

The air stream passing a blade element of height Δr will exert upon this blade element a force Δk. One component Δk_y is acting in the direction of the axis or vertically to the disk. The other component Δk_x is acting in the direction of rotation, Fig. 2. The sum of the blade components in the elementary ring area f_r' is represented by the following equations:

$$k_x = \sum \Delta k_x, \qquad k_y = \sum \Delta k_y, \qquad \Delta \mathbf{k} = \Delta \mathbf{k}_x + \Delta \mathbf{k}_y.$$

Further the axial thrust on f_r' is equal to the pressure difference at the disk, so that the following equation holds:

[6] $$k_y = (p_r' - p_r'')f_r'.$$

The energy of the wind transferred to the elementary area f_r' is:

[7] $$e_r = k_x u_r.$$

Taking into account formula [7], it is possible to use Bernoulli's formula for the absolute velocities before and behind the mill disk:

$$[p_r' + \rho/2 \cdot (v_r')^2]v_r' f_r = [p_r'' + \rho/2 \cdot (v_r')^2 + \rho/2 \cdot o_r^2]v_r' f_r' + e_r + \tau' v_r' f_r';$$

[8] $$e_r = k_x u_r = v_r' f_r' (p_r' - p_r'' - \rho/2 \cdot o_r^2 - \tau).$$

Each elementary air particle of the air stream between f_1 and f_r, Fig. 1, enters this elementary air cone at f_1 with the velocity v_1 and pressure p_0 and leaves this cone at f_r at the velocity v_r and same pressure p_0. The air mass between f_1 and f_r is ΔM and its volume ΔV. The air particle needs t seconds to travel that distance. The velocity of this mass is retarded from v_1 to v_r by a force that operates in the direction of the axis. The mean value of this force is given by Newton's formula

$$k_y' = \frac{\Delta M}{g}\left(\frac{v_1 - v_r}{t}\right) \quad \text{or} \quad k_y' = \frac{\gamma}{g}\frac{\Delta V}{t}(v_1 - v_r).$$

Volume ΔV passes in t seconds the elementary area f_r' so that:

$$\Delta V/t = f_r' v_r' \text{ and } k_y' = \rho f_r' v_r' (v_1 - v_r).$$

This retardant force must have, according to Newton's law, a reactive force of the same value in the mill disk, so that:

$$k_y' = k_y \text{ and therefore } f_r'(p_r'-p_r'') = \rho f_r' v_r'(v_1-v_r),$$

[9]
$$p_r'-p_r'' = \rho v_r'(v_1-v_r).$$

Subtraction of formula [4] from formula [3] gives:

[10] $$p_r'-p_r'' = \rho/2\cdot(v_1^2-v_r^2).$$

Substitution of formula [9] into [10] gives:

[11] $$v_r' = \tfrac{1}{2}(v_1+v_r).$$

Substitution of formula [10] into [8] gives:

[12] $$e_r = k_x u_r = \rho/2\cdot v_r' f_r'(v_1^2-v_r^2-o_r^2-2\tau/\rho).$$

Substitution of formula [5] into [8] gives:

[13] $$e_r = k_x u_r = \rho/2\cdot v_r' f_r'(-2o_r u_r),$$

[14] $$k_x = \rho/2\cdot v_r' f_r'(-2o_r).$$

From equations [12] and [13] it is possible to calculate o_r (u_r is negative, Fig. 3, $u_r = -m_r v_1$):

[15] $$o_r = u_r \pm (u_r^2+v_1^2-v_r^2-2\tau/\rho)^{\frac{1}{2}}.$$

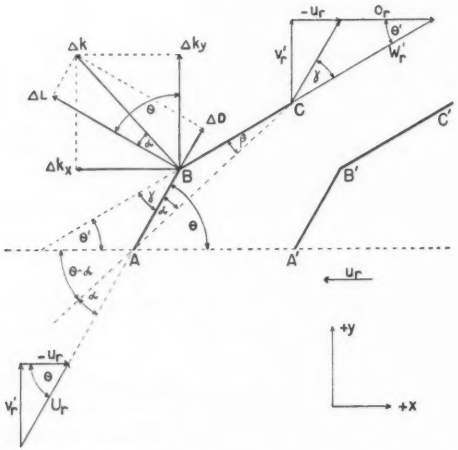

FIG. 3. Forces on the blade at the distance r from the axis.

It is now possible to calculate e_r maximum. The condition for a maximum is $de_r/dv_r = 0$ and formula [13] gives the following equation:

[16] $$\frac{de_r}{dv_r} = \rho f_r'(-u_r)\left[\frac{do_r}{dv_r}\, v_r' + o_r \frac{dv_r'}{dv_r}\right] = 0.$$

From formula [11]: $dv_r'/dv_r = \frac{1}{2}$.
From formula [15]: $do_r/dv_r = \frac{1}{2}(u_r^2-v_1^2-v_r^2-2\tau/\rho)^{-\frac{1}{2}}(-2v_r)$.

The final form of equation [16], after substitutions, is:

[17] $$(-2v_r^2-v_rv_1+u_r^2+v_1^2-2\tau/\rho)^2 = u_r^2(u_r^2+v_1^2-v_r^2-2\tau/\rho).$$

In a design, the tip speed ratio to wind velocity is always given (n). Further m_r and x_r are defined as follows:

$$m_r = n\,r/R, \qquad u_r = -m_rv_1 = u_R\,r/R, \qquad x_r = v_r/v_1.$$

After these substitutions, formula [17] takes a more convenient form:

[18] $$(-2x_r^2-x_r+m_r^2+1-2\tau/\rho v_1^2)^2 = m_r^2(m_r^2+1-x_r^2-2\tau/\rho v_1^2).$$

An ideal mill is an extreme case; it does not deflect the air stream, $o_r = 0$, and formula [15] may be written as:

$$0 = \frac{v_1^2}{u_r^2}-\frac{v_r^2}{u_r^2}-\frac{2\tau}{\rho u_r^2}.$$

Both sides of the equation are equal in case of $u_r \to \infty$. Practically this means very high velocity at the tip of the blade. Tip speeds up to $|u_R| = 10v_1$ are possible, but the starting torque of such a mill is already so low that it will not start at all at lower wind speeds. Division of the second power in formula [18] by $m_r^2 \to \infty$ will give as result ($\tau = 0$)

$$-3x_r^2-2x_r+1 = 0, \qquad x_r = v_r/v_1 = \tfrac{1}{3}, \qquad v_r = \tfrac{1}{3}v_1.$$

Assuming that $o_r = 0$ and $\tau = 0$, formula [12] is converted into the classic formula for the energy available at the "ideal mill"

$$E = \sum e_r = \rho/2 \cdot v' F'(v_1^2-v_r^2), \qquad F' = \sum f'.$$

Taking into account formula [11] a maximum is found for $v_r = \frac{1}{3}v_1$

[19] $$\text{id } E_{\max} = 16/27 \cdot \rho/2 \cdot F'v_1^3.$$

The energy in the air, supposing that the disk has been removed, is:

$$\text{tot } E = \rho/2 \cdot v_1^3 F'.$$

The efficiency of an "ideal mill" is therefore

$$\eta_{\text{id}} = 16/27.$$

Comparing the removed wind energy with the energy entering area F_1 the "true" efficiency will be ([1] and [11]):

$$\eta_{\text{tr}} = 8/9 = \text{id } E_{\max}/E_1, \qquad E_1 = \rho/2 \cdot F_1v_1^3 = \rho/2 \cdot \tfrac{2}{3}F'v_1^3.$$

The axial thrust is given by formula [6], and in the case of $E_{\max}$ the thrust of an "ideal mill" will be:

$$\sum k_y = K_y = (p'-p'')\,F' = \rho/2 \cdot (v_1^2-v_r^2)F',$$

[20]

$$K_y = 8/9 \cdot \rho/2 \cdot F'v_1^2.$$

Another extreme case is presented by $u_r = 0$ and $m_r = 0$ when formula [18] is converted to:

$$2x^2+x-1 = 0, \qquad x = v_r/v_1 = \tfrac{1}{2}, \qquad v_r = \tfrac{1}{2}v_1.$$

From formula [15]: $o_r = \tfrac{1}{2}v_1\sqrt{3}, \qquad v_r' = \tfrac{3}{4}v_1.$

From formula [12]: $e_r = 0.$

A mill constructed for zero speed $u_r = 0$ has the highest possible torque. Formula [23] gives its value as:

$$T = 2\pi \cdot \rho/2 \cdot \tfrac{3}{4}\sqrt{3} \cdot v_1^2 \int_{r_0}^{R} r^2 dr.$$

Both extreme cases show that all x values, calculated from formula [18], must be in the range

[21] $$\tfrac{1}{3} < x < \tfrac{1}{2}.$$

The ratio of the energy output of an elementary ring area f_r' to the energy output of an "ideal mill" in the same area is the efficiency η_r of that area at the distance r and height Δr ([13]; [19]):

[22] $$\eta_r = \frac{\max e_r}{\max e_{id}} = \frac{27}{16}\frac{v_r'}{v_1^3}(-2o_r u_r).$$

The torque of an elementary ring area is given by formula [14] as

$$t_r = k_z r = r f_r' v_r' \cdot \rho/2 \cdot (-2o_r), \text{ or}$$

[23] $$t_r = 4\pi \cdot \rho/2 \cdot v_r'(-o_r) r^2 \Delta r.$$

THEORY OF THE AIRFOIL

Nomenclature

α_r—Angle of attack, represented by vector U_r and chord AC.
β_r—Angle of leave, represented by vector W_r and chord AC.
γ_r—Angle of deflection of the air stream; $\gamma_r = \alpha_r + \beta_r$.
θ_r—Pitch of the blade part AB.
θ_r'—Pitch of the blade part BC.
$\theta_r - \alpha_r$—Pitch of the chord AC.
l_r—Length of the blade chord AC at radius r (m.).
d_r—Distance between two blades (AA') at radius r (m.).
a_r—Density of blades.
z—Number of blades.
$\Delta f_r''$—Area of one blade element at radius r and of height Δr(m.^{2}).
f_r''—Area of z blade elements at radius r and of height Δr (m.^{2}).
ΔL—Lift of one blade element (kgm.).

ΔD—Drag of one blade element (kgm.).
c_L—Lift coefficient.
c_D—Drag coefficient.

In order to get the maximum possible energy output and torque from a low-speed windmill, the airfoil blades must be so designed that they give to the air stream the theoretically required deflection o_r, at a predetermined value of n ([14]; [15]). In other words, the task of an airfoil blade is to bend or deflect an air stream of certain depth by a theoretically given angle γ.

Fig. 3 shows a blade element of height Δr at distance r from the axis. It is slightly curved at point B but drawn as a broken line ABC. The pitch of the blade parts AB and BC is such that the following equations hold for the angles θ_r and θ_r':

[24] $$\tan \theta_r = v_r'/(-u_r),$$

[25] $$\tan \theta_r' = v_r'/(-u_r+o_r),$$

[26] $$\gamma_r = \theta_r-\theta_r'.$$

According to tests, the force Δk of a deflected air stream upon a good blade should be vertical to the blade chord AC so that:

$$\tan(\theta_r-\alpha_r) = -\Delta k_x/\Delta k_y.$$

The above equation holds because $\Delta k \perp AB$ and $\Delta k_y \perp u_r$ and the angle between Δk and Δk_y is $\theta_r-\alpha_r$.

The following equation, obtained by using formulas [5], [6], and [12], holds for the pitch of the chord AC:

[27] $$\tan(\theta_r-\alpha_r) = v_r'/(-u_r+\tfrac{1}{2}o_r).$$

Parts AB and BC of the blade at the radius r are defined by the following trigonometrical formulas:

[28] $$AB = l_r \sin \beta_r/\sin \gamma_r, \qquad BC = l_r \sin \alpha_r/\sin \gamma_r.$$

Formulas [24] to [28] determine the shape and position of the airfoil. α_r is predetermined and should not be chosen arbitrarily (3) or constant over the whole radius of about three degrees (7). The depth of the chord determines only the depth of the air stream to be deflected and not the angle of deflection. Only the correct shape of the blade gives the correct angle of deflection and thus maximum energy and torque and not excessively long chords.

It is common to express the lift and drag as follows:

[29] $$\Delta L = c_L \cdot \rho/2 \cdot \Delta f_r'' U_r^2, \qquad \Delta D = c_D \cdot \rho/2 \cdot \Delta f_r'' U_r^2.$$

Further the following relations hold (Fig. 3):

[30] $$\Delta k^2 = \Delta k_x^2+\Delta k_y^2 = \Delta L^2+\Delta D^2 \text{ (for one blade element)},$$
$$k^2 = k_x^2 + k_y^2 = L^2 + D^2 \text{ (for } z \text{ blade elements)}.$$

By using formulas [5], [6], [14], and [29], formula [30] can be written as follows:

$$(\rho/2)^2(f_r'')^2\ U_r{}^4(c_L{}^2+c_D{}^2) = (v_r')^2(f_r')^2(\rho/2)^2 4o_r{}^2+(f_r)^2(\rho/2)^2o_r{}^2(o_r-2u_r)^2.$$

Further, formulas [5] and [10] give the following equation:

$$o_r{}^2(o_r-2u_r)^2 = (v_1{}^2-v_r{}^2)^2.$$

When this equation is substituted into formula [30], the final form of [30] becomes

$$[31] \qquad \frac{(f_r'')^2}{(f_r')^2} = \frac{(v_r')^2 4\ o_r{}^2+(v_1{}^2-v_r{}^2)^2}{U_r{}^4(c_L{}^2+c_D{}^2)} = \frac{l_r{}^2}{d_r{}^2} = a_r{}^2.$$

The depth l_r of the chord AC is determined by the following formula:

$$[32] \qquad l_r = a_r.2\pi r/z.$$

The number of blades is generally chosen so that the ratio of blade length to average depth of chord is about five.

The value of a_r [31] depends upon $c_L{}^2+c_D{}^2$; c_L and c_D are experimentally determined constants. Approximate values from the literature (2) will give either too long chords (this means useless weight) or too short chords (this means that only part of the air stream has the deflection γ_r) decreasing the efficiency and torque. Straight-line multiblade cascades representing the chosen elementary zones must be tested in the wind tunnel.

All derived formulas can be used for the calculation of high-speed mills. Profiles for the sections of the "propeller blade" must be chosen in accordance with the theoretical deflection γ_r.

Further it is necessary to show that the distances between AB and $A'B'$, and BC and $B'C'$ correspond to the relative air velocities between these parts, so that there is no radial shift of the air stream due to the geometrical properties of the cascade (Fig. 4).

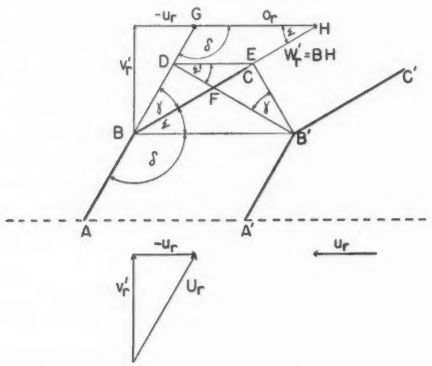

FIG. 4. Relation between blade distances and wind velocities.

$B'D$—Distance between AB and $A'B'$; further $U_r \perp B'D$.
$B'E$—Distance between BC and $B'C'$; further $W_r' \perp B'E$.

If there is no radial flow, that is a flow vertical to AA' (Fig. 4), the following equation in accordance with formula [1] must hold:

$$U_r(B'D)\Delta r = W_r'(B'E)\Delta r; \quad \text{or} \quad \frac{B'D}{B'E} = \frac{W_r'}{U_r} = \frac{BH}{BG}.$$

Equal angles are ϵ and ϵ, δ and δ because they are angles between parallel lines, and γ and γ because they are angles between vertical lines. Further it is possible to connect points B, B', E, D by a circle of the diameter BB' because the angle at E is 90° and the angle at D is 90°. Therefore

$$\triangle BFB' \backsim \triangle DEF \text{ and } \epsilon' = \epsilon;$$
$$\triangle B'ED \backsim \triangle BHG;$$

and hence $$B'D/B'E = BH/BG.$$

CALCULATIONS

In order to design a low-speed mill, it is sufficient to make all necessary calculations for a limited number of chosen zones; for example in a manner shown by Fig. 5. The reason for this method is that general formulas for the variables (as functions of r, v_1, n) would be too complicated.

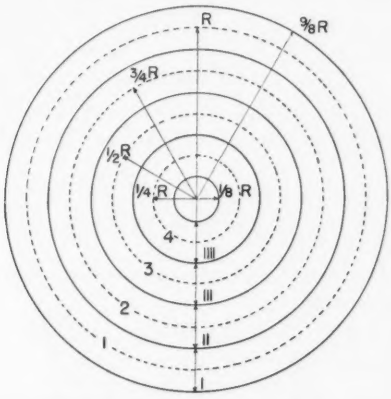

FIG. 5. Subdivision of the disk.

Circles 1, 2, 3, 4 represent chosen elementary ring areas with radius r equal to R, $\frac{3}{4}R$, $\frac{1}{2}R$, $\frac{1}{4}R$, respectively. Calculated values found for elementary ring areas 1, 2, 3, 4 are applied to the disk zones I, II, III, IIII correspondingly. All calculated values are tabulated in Table I in the order in which the calculations were made. The "Multiplication factor" contains the radius of the disk but in the manner shown by Fig. 5. The "Variable" is equal to "Multiplication factor" times "Constant of the zone".

TABLE I

TABLE OF RESULTS

Variable	Formula	Units	Multiplication factor	Constant of the zone				Constant of the disk
				I	II	III	IIII	
r	—	Meter (m.)	1	R	$\frac{3}{4}R$	$\frac{1}{2}R$	$\frac{1}{4}R$	—
m_r	—	—	1	1	$\frac{3}{4}$	$\frac{1}{2}$	$\frac{1}{4}$	—
u_r	—	m./sec.	$-v_1$	1	$\frac{3}{4}$	$\frac{1}{2}$	$\frac{1}{4}$	—
x_r	18	—	1	0.37	0.38	0.40	0.44	—
v_r	18	m./sec.	v_1	0.37	0.38	0.40	0.44	—
v_r'	11	m./sec.	v_1	0.68	0.69	0.70	0.72	—
o_r	15	m./sec.	v_1	0.36	0.44	0.54	0.68	—
Zone area	—	m.^{2}	πR^2	0.500	0.375	0.250	0.125	1.25
e_r	13	m-kgm./sec.	$\pi\rho R^2 v_1^3$	0.123	0.085	0.047	0.015	0.27
η_r	22	%	1	83	77	64	41	73
l_r	23	kgm.m.	$\pi\rho R^3 v_1^2$	0.123	0.085	0.047	0.015	0.27
$p_r' - p_r''$	10	kgm./m.^{2}	$\rho/2 \cdot v_1^2$	0.863	0.856	0.840	0.806	—
k_y	6	kgm.	$\pi \cdot \rho/2 \cdot R^2 v_1^2$	0.43	0.32	0.21	0.11	1.07
θ_r	24	deg.	1	34.3	42.6	54.5	70.7	—
θ_r'	25	deg.	1	26.6	30.0	33.9	37.8	—
γ_r	26	deg.	1	7.7	12.6	20.6	32.9	—
$\theta_r - \alpha_r$	27	deg.	1	29.9	35.4	42.3	50.7	—
α_r	—	deg.	1	4.4	7.2	12.2	20.0	—
U_r	2	m./sec.	v_1	1.21	1.02	0.86	0.76	—
$\sqrt{(c_L^2 + c_D^2)}$	—	—	1	0.6	0.8	1.0	1.2	—
a_r	31	—	1	1.13	1.25	1.52	1.82	—
l_r	32	m.	$2\pi R/z$	1.13	0.94	0.76	0.45	—
AB	28	m.	l_r	0.43	0.43	0.40	0.40	—
BC	28	m.	l_r	0.57	0.57	0.60	0.63	—

DISCUSSION

1. Values calculated for v_r and v_r' show that there is very little radial variation in air velocity along the disk radius. These velocities may be regarded as constant.

2. The axial thrust, represented by $p_r' - p_r''$, is practically constant along the radius. This means that there is no radial shift of the air stream due to differences in pressure in the disk.

3. The total axial thrust of an ideal mill at maximum energy output will be, according to formula [20]:

$$K_y = 8/9 \cdot \rho/2 \cdot v_1^2 \pi[(9/8)^2 R^2 - (1/8)^2 R^2]$$
$$= \rho/2 \cdot \pi R^2 v_1^2 \times 1.11.$$

The total axial thrust of the low-speed mill is, from Table I, with close approximation

$$K_y = \rho/2 \cdot \pi R^2 v_1^2 \times 1.07.$$

There is practically no difference in thrust between the ideal mill and the low-speed mill.

4. The efficiency η_r of the elementary ring areas varies considerably, from 83% at the tip to 41% at the hub. In order to get the average efficiency, it is necessary to calculate the energy output for the ideal mill and for the low-speed mill.

$$\max E_{1d} = \pi[(9/8)^2R^2 - (1/8)^2R^2]16/27 \cdot \rho/2 \cdot v_1^3$$
$$= \pi R^2 \rho v_1^3 \times 0.37.$$

The total energy output of the low-speed mill from Table I will be with close approximation:

$$\max E_{1spd} = \pi R^2 \rho v_1^3 \times 0.27.$$

Thus the theoretical efficiency that cannot be exceeded is:

$$\eta_{1spd} = 0.73.$$

5. Example for the design of a blade: Tip speed of the wind turbine is equal to the wind velocity ($n = 1$). Diameter of the disk = 2.8 m. ($9/8\,R$) (about nine feet). Diameter of the hub = 0.3 m. Free length of the blade = 1.25 m. Number of blades $z = 24$. Distance between two blade tips = 0.367 m. See Fig. 5.

The shape or profile of the blade varies with the blade radius r. At a certain distance r from the axis it is determined by the angles θ_r and θ_r' and by the chord parts AB and BC of the chord AC (see Figs. 3, 5, 6). Four r values may be regarded as sufficient to determine the blade.

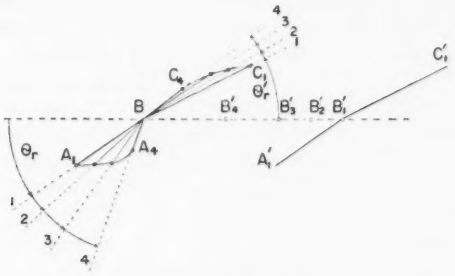

FIG. 6. Radial view of the blade.

Zone	r (m.)	θ_r (deg.)	θ_r' (deg.)	$AC = l_r$ (m.)	AB (m.)	BC (m.)
I	$R = 1.25$	34.3	26.6	0.37	0.16	0.21
II	$\frac{3}{4}R = 0.94$	42.6	30.0	0.31	0.13	0.18
III	$\frac{1}{2}R = 0.62$	54.5	33.9	0.25	0.10	0.15
IIII	$\frac{1}{4}R = 0.31$	70.7	37.8	0.15	0.06	0.09

Fig. 5 shows the r values chosen. Fig. 6 represents the blade viewed from the tip, in the direction of its length or radius. The line of break goes vertically through point B. Blades may have a sharp break or they may be slightly curved around B.

Tests on "broken blades" were carried out at the University of Askov in Denmark by Prof. La Cour, and recommended by him for windmills (7).

REFERENCES

1. CONRAD, W. Forschung, 8 (1): 2. 1937.
2. CURRY, M. Die Aerodynamik des Segels und die Kunst des Regatta-Segelns. Huber und Diessen Verlag, München.
3. FALES, E. N. Windmills. Marks, Mechanical Engineers Handbook. McGraw-Hill Book Company, Inc., New York. 1951.
4. GOLDING, E. W. Research (London), 6 (4): 138. 1953.
5. PARSONS, H. E. Eng. J. (Can.), 36 (1). 1953.
6. PUTNAM, P. C. Power from wind. D. Van Nostrand Company, Inc., New York. 1948.
7. VAN HEYS, J. W. Wind und Windkraftanlagen. Georg Siemens Verlag, Berlin. 1947.

DENSITY EFFECTS IN THE RAMAN SPECTRUM OF AMMONIA[1]

By C. A. Plint,[2] R. M. B. Small,[3] and H. L. Welsh

ABSTRACT

The Raman spectra of ammonia as a high pressure gas, liquid, solid, and aqueous solution are compared with the spectrum of the low pressure gas. At gas pressures up to 80 atm. no appreciable hindering of rotation is present; a weak satellite of the ν_1 band is an unexplained feature of the spectrum at high pressure. The spectra of the liquid, solid, and aqueous solution are interpreted without postulating dimerization; the three higher frequency maxima can be assigned to the $2\nu_4$, ν_1, and ν_3 vibrations if it is assumed that hindering of rotation is almost complete. The rotational fine structure found by early workers for the aqueous solution could not be observed even at high dispersion.

INTRODUCTION

The Raman spectrum of a substance in a condensed phase often shows considerable differences from the spectrum of the same substance as a low pressure gas. The differences, which are caused by intermolecular forces, are usually small for nonpolar molecules but can be large for strongly polar molecules such as water and ammonia. The Raman spectrum of ammonia, the subject of the present investigation, has been studied frequently in the liquid, the solid, and aqueous solutions. However, some of the interpretations of the spectra appear unconvincing in the light of the present more complete knowledge of the spectrum of the free molecule.

For liquid ammonia at −40°C. Daure (5) observed three Raman lines of nearly equal intensities at displacements 3210, 3310, and 3380 cm^{-1}. For the liquid at room temperature Bhagavantam (2) reported the same lines but with different relative intensities, the outer lines of the triplet being less intense than the central line. At this time investigations of the gas had revealed only the symmetric vibration ν_1 ($\Delta\nu$ = 3334 $cm.^{-1}$) in this region. Bhagavantam therefore conjectured that the line for the liquid at 3310 $cm.^{-1}$ is due to ν_1 and that the other two lines are caused by the splitting of the ν_1 frequency in a dimer $(NH_3)_2$, whose concentration relative to that of the single molecule decreases as the temperature is raised.

In solid ammonia at −190°C. Sutherland (13) observed two lines at displacements 3203 and 3369 $cm.^{-1}$, which he attributed to the dimer. He assumed that the dimerization is complete in the solid since he found no trace of a band corresponding to ν_1 of the free molecule.

The spectrum of aqueous solutions of ammonia also shows a triplet, but according to Langseth (8) a fine structure is present in the outer components. The fine structure was confirmed by Hollaender and Williams (7). Since the pattern of discrete lines agreed with the rotational Raman spectrum and the

[1]*Manuscript received April 29, 1954.*
Contribution from the McLennan Laboratory, University of Toronto, Toronto, Ontario.
[2]*Holder of a Postgraduate Dominion Travelling Scholarship of the Worshipful Company of Goldsmiths, London, England, 1950–52, and a Scholarship of the Research Council of Ontario, 1952–53. Present address: Department of Physics, University of Oklahoma, Norman, Okla., U.S.A.*
[3]*Present address: Research and Development Division, Polymer Corporation Ltd., Sarnia, Ontario.*

ν_1 rotation–vibration band in the infrared, the outer components of the triplet were interpreted as rotational wings of the ν_1 band. However, a rotational fine structure implies the existence of free molecular rotation in the solution—a surprising result since the interactions between the molecules of water and ammonia should be very large. More recent investigations by Daure, Kastler, and Berry (6) and by Marchand (11) have not corroborated the fine structure found by the earlier workers.

The Raman spectrum of the gas is now known in some detail. In addition to the sharp Q branches of the ν_1 band ($\Delta\nu = 3334$ cm.$^{-1}$) and the overtone $2\nu_4$ ($\Delta\nu = 3219$ cm.$^{-1}$) (9), the region of higher frequency Raman shifts shows an extensive band with rotational structure extending from 3200 to 3700 cm.$^{-1}$, which can be attributed to the doubly degenerate ν_3 vibration (4). The origin of the band as determined from the analysis is at $\Delta\nu = 3444$ cm.$^{-1}$, and corresponds to a minimum of intensity since the Q branch is split into various subbranch lines which do not coincide in frequency (Fig. 1(*a*)). No rotational wings were observed for the ν_1 band indicating that the band is highly polarized.

An obvious interpretation of the spectrum of the liquid is the assignment of the three maxima, in order of increasing Raman displacement, to $2\nu_4$, ν_1, and ν_3, the latter band showing in contrast to the gas a sharp maximum at the band origin because of hindering of rotation. Also, the presence of discrete rotational lines in the wings of the ν_1 band for the aqueous solution now appears very doubtful since no such structure is observed for the gas. The present investigation of the high pressure vapor, liquid, solid, and aqueous solution was carried out with the aim of clarifying these points.

THE RAMAN SPECTRUM OF AMMONIA VAPOR AT HIGH PRESSURE

To follow continuously the changes in the Raman spectrum with increasing density an attempt was made to observe the spectrum of the vapor up to and beyond the critical point.* The ammonia was contained in a fused quartz tube, 5 mm. in internal diameter, with a wall thickness of about one millimeter. The tube was divided by an offset constriction, serving as a light trap, into an illuminated section, 10 cm. long, and a reservoir section. A small bulb carefully blown on the end of the illuminated section was the exit window for the scattered light. Ammonia was introduced by a low temperature distillation into the tube, which was then sealed off. The illuminated section and the reservoir containing the liquid were heated independently, the former by hot air passing through a fused quartz jacket, the latter by a coil of nichrome wire. In the experiments the illuminated section was kept at about 135°C. and the reservoir at a series of lower temperatures to produce different vapor densities. The Raman spectrum was excited by Hg2537 radiation from a helical quartz mercury lamp with water-cooled electrodes, and was photographed with a Hilger E2 spectrograph. Eastman 103a0 spectroscopic plates, calibrated for intensities with a stepped slit and a low voltage hydrogen arc, were used.

Spectrograms were obtained in the pressure range from 38 to 80 atm. During the exposure at the highest pressure the Raman tube exploded, although it

**At the critical point, 132.4°C., the pressure is 111.5 atm. and the density 292 Amagat units.*

had been tested previously at higher pressures. This spectrogram showed the vibrational lines of hydrogen and nitrogen, indicating that considerable decomposition of ammonia had taken place. It is probable that the decomposition was caused by Hg1850 radiation and was accelerated by the elevated temperature in the illuminated part of the tube.

From the spectrograms obtained it was found that the relative intensity profile in the region 3200–3700 cm.$^{-1}$ showed no observable change in the density range 38–110 Amagat units. The microphotometer tracing reproduced in Fig. 1(*b*) shows, in addition to the comparatively sharp lines ν_1 and $2\nu_4$, a broad band of the same general shape and extent as the ν_3 band in the low pressure gas (Fig. 1(*a*)). The band origin is indicated by a minimum of intensity

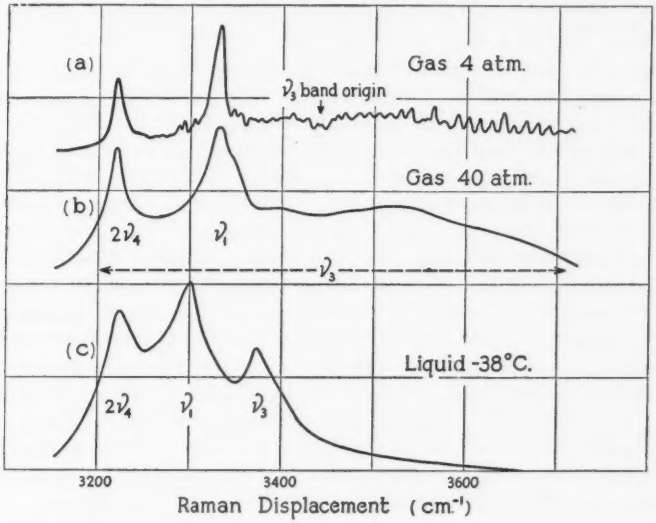

FIG. 1. Raman spectra of ammonia. (*a*) Microphotometer tracing for the gas at 4 atm. (*b*) Microphotometer tracing for the gas at 40 atm. (*c*) Intensity profile for the liquid at −38°C.

but no fine structure is present. It is therefore concluded that, although the fine structure is no longer apparent because of collision broadening, the molecular rotation is not appreciably hindered at densities up to 110 Amagat units. The effect of higher densities might be observed by using visible excitation; however, it did not appear worth while to continue the investigation of the high pressure vapor since the observations on liquid and solid ammonia discussed below seemed to permit a unique interpretation.

An interesting feature of the spectrum at high vapor densities is a new line which appears on the side of the ν_1 line towards higher frequency shifts. This satellite line can be seen on the microphotometer tracing in Fig. 1(*b*) as a shoulder on the ν_1 line. In a spectrogram obtained at a pressure of 31 atm. on a spectrograph with a dispersion about five times as great as the Hilger E2

instrument the satellite appears as a fairly well resolved line at a Raman shift of 3351 $\pm$ 2 cm^{-1}. Since there is no corresponding line in the spectrum at low pressure, the new line must be caused by some density effect whose nature is not yet clear.

THE RAMAN SPECTRUM OF LIQUID AMMONIA

The Raman spectrum of the liquid phase was studied at several temperatures between the normal boiling point, -34°C., and -70°C.

The essential feature of the Raman tube, which has been described (3), is that the substance tube is surrounded by a refrigerant chamber but separated from it by a vacuum space. Anhydrous ammonia was condensed in the tube using solid carbon dioxide and acetone as the refrigerant. The temperature of the liquid was estimated from the vapor pressure measured on a mercury manometer. Hg4358 radiation from a helical mercury arc with water-cooled electrodes was used for excitation, and the relative intensities in the Raman spectrum were measured directly with a photoelectric recording spectrograph (10). The Raman shifts were obtained from the dispersion curve of the spectrograph using Hg5025.6 as a reference point in the region of the Raman lines.

The measured displacements of the three maxima are 3218, 3300, and 3373 cm.$^{-1}$, with an estimated error of ± 3 cm^{-1}. In Fig. 1 the intensity contour of the spectrum of the liquid at -38°C. is compared with microphotometer tracings of the spectrum of the gas. If the intensity of the ν_3 band in the gas is imagined to be concentrated at the band origin, as it would be if molecular rotation were absent, the similarity of the gas and the liquid spectra is very marked. The frequencies of the ν_1 and ν_3 bands are shifted towards lower values in the liquid as is usual for polar molecules. The $2\nu_4$ band does not show a large change in frequency probably because of the altered conditions in the Fermi resonance to which it owes its intensity. This interpretation of the spectrum is in accordance with polarization measurements in the liquid by Bhagavantam (2) and by Daure *et al.* (6) who showed that the two lower frequencies are polarized and the higher frequency is depolarized.

Intensity profiles of the spectrum of the liquid at several different temperatures are shown in Fig. 2; these have been matched at the central maximum to show more clearly the relation between the relative intensities of the lines and the temperature. As noted by Bhagavantam the peak intensities of the outer lines of the triplet increase relative to that of the central line as the temperature is lowered. A closer examination of the contours shows that this variation of the peak intensities is probably caused by changes in the half-widths of the bands; in particular, the ν_1 band appears to become broader and the ν_3 band sharper as the temperature is lowered. An attempt was therefore made to divide the contour into its three component bands. The procedure used is at first sight somewhat arbitrary but, when considered in conjunction with the results given below on the solid, has some justification.

It is assumed that the main effect of increasing density on the ν_3 band is an increasing hindering of the rotation so that, at liquid densities, the discrete rotational levels associated with each of the vibrational levels are replaced by

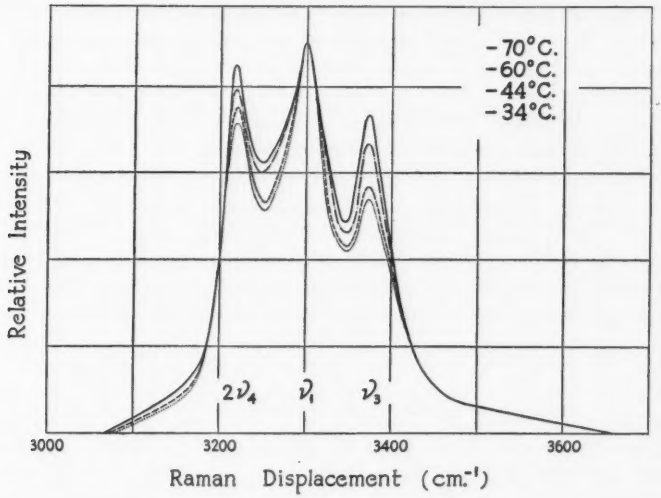

FIG. 2. Intensity profiles of the Raman spectrum of liquid ammonia at various temperatures.

a continuum of librational levels. The ratio of the intensities for frequency displacements $\delta\nu$ and $-\delta\nu$ from the peak of the band would therefore be equal to $\exp(hc\delta\nu/kT)$. The intensity in the spectrum beyond the Raman displacement $\Delta\nu = 3400$ cm.$^{-1}$ was accordingly ascribed wholly to ν_2 and the contour of the band calculated according to this intensity relation. The contour obtained, shown by a dotted line in Fig. 3, is asymmetric and degraded towards greater Raman displacements, and is very similar to the contour of the solid (Fig. 5) where the ν_3 band is much better resolved. The half-widths of the ν_3

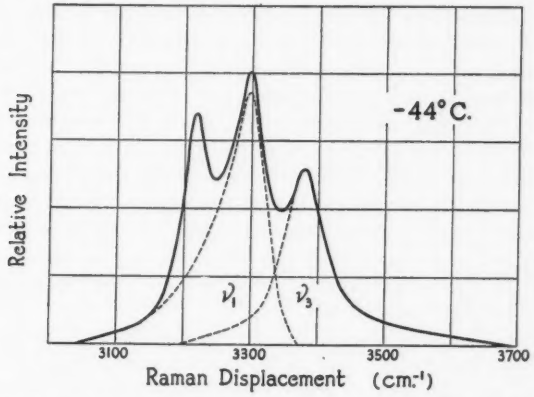

FIG. 3. Division of the intensity profile of the liquid spectrum into components.

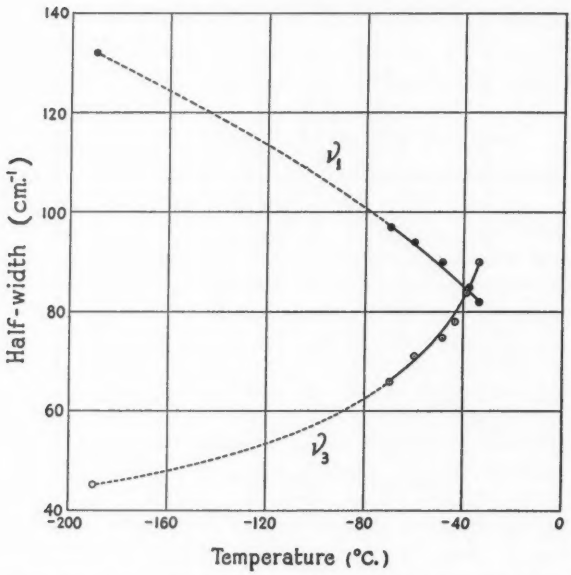

FIG. 4. Graph of the half-widths of the ν_1 and ν_3 bands of liquid ammonia in the temperature range −34°C. to −70°C. and of solid ammonia at −190°C.

band, separated out by the above procedure, are plotted against the temperature of the liquid in Fig. 4. The graph shows a decreasing half-width with decreasing temperature and can be extrapolated by a smooth curve to include the value for the solid at −190°C. The observed variation of the half-width is thus in accordance with the assumption of hindered rotation in the liquid; also, the small value of the measured half-width compared with the extent of the band in the gas shows that the hindering of rotation is almost complete.

In Fig. 3 the residual intensity, after the separation of the component ν_3, has been divided into two parts attributed to $2\nu_4$ and ν_1, the division being carried out so that the ratio of the intensities of $2\nu_4$ and ν_1 is approximately the same as in the low pressure gas. In Fig. 4 the half-widths of the ν_1 component thus obtained are plotted against the temperature; in contrast to the ν_3 band the half-width of the ν_1 band increases with decreasing temperature. The contour of the ν_1 component shows a considerable asymmetry and is strongly degraded towards lower frequency shifts. This shape is very similar to that which has been found for the ν_1 band of steam at high pressures (1), and might be taken to be typical of the effect of high densities on a symmetrical vibration of a strongly polar molecule.

The effect of increasing density on the Raman spectrum is very different for nonpolar and polar molecules. It has been shown that for methane, for example, no broadening of the ν_1 Raman line, which is entirely due to isotropic scattering, is observed even in the liquid (3); for ammonia and water on the

other hand, the broadening of the ν_1 line is very pronounced at high densities. This behavior of the symmetric frequencies of polar molecules is probably related to the coupling of the vibrations in pairs of molecules interacting as in the Keesom orientation effect. The contour of the triply degenerate ν_3 band in liquid methane shows that there is no appreciable hindering of the rotation at high densities (3). However, in ammonia hindering of rotation is very pronounced in the liquid and is responsible for the line-like appearance of the ν_3 band.

From the foregoing discussion it is therefore concluded that the Raman spectrum of liquid ammonia can be explained essentially in terms of the different effects of the intermolecular forces on the ν_1 and ν_3 bands. In particular, dimerization need not be postulated to account for the spectrum.

THE RAMAN SPECTRUM OF SOLID AMMONIA

The experimental arrangement for solid ammonia was similar to that employed for the liquid. Ammonia was condensed as a liquid in the Raman tube using liquid air as the refrigerant; the vacuum space between the refrigerant and the sample ensured slow cooling so that a fairly clear crystalline solid was obtained. A thermocouple embedded in the solid was used to measure the temperature.

A recorder tracing of the spectrum excited by Hg4047 with the solid at -190°C. is shown in Fig. 5(*a*). The two pronounced maxima at measured

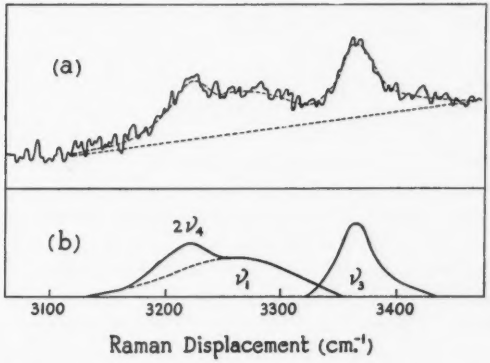

FIG. 5. Raman spectrum of solid ammonia at -190°C. (*a*) Recorder tracing. (*b*) Division of intensity profile into components.

Raman displacements 3220 and 3365 cm.$^{-1}$ are those observed by Sutherland (13). However, from the shape of the intensity contour there is no doubt that a third, very broad, component lies between the two sharper maxima. In Fig. 5(*b*) the intensity profile has been divided into three components, the central one having a maximum at 3265 $\pm$ 10 cm^{-1}. This broad central component can therefore be identified with the symmetric frequency ν_1, while the

other two maxima can be attributed to $2\nu_4$ ($\Delta\nu = 3220$ cm.$^{-1}$) and ν_3 ($\Delta\nu = 3365$ cm.$^{-1}$). Thus the spectrum is essentially the same as that of the liquid.

The measured half-widths of ν_1 and ν_3 are 132 and 45 cm.$^{-1}$ respectively, and these values, as has been pointed out above, fit an extension of the half-width versus temperature graphs for the liquid (Fig. 4). However, it is probable that, at least in the case of the ν_1 band, the half-width is not a function of the temperature alone and increases on passing to the solid state. Unfortunately, the transition from the liquid to the solid at the normal freezing point could not be studied with the arrangement used.

In a recent investigation of the infrared spectrum of solid ammonia Reding and Hornig (12) concluded that there is no evidence of dimerization in the solid. The present study of the Raman spectrum confirms this view. However, these authors' assignment of the three infrared bands in the 3200–3400 cm.$^{-1}$ region to ν_1, $2\nu_4$, and ν_3 in order of increasing frequency is not the same as that adopted here. When integrated rather than peak intensities are considered, the relative intensities of the three Raman bands do not change to any marked extent with change of state. An examination of the infrared absorption curves of Reding and Hornig shows that the integrated infrared intensities also show no marked change from the gas if the broad maximum at 3297 cm.$^{-1}$ is assigned to ν_1. Furthermore, if the corresponding broad maximum at 2390 cm.$^{-1}$ in the infrared spectrum of heavy ammonia is assigned to ν_1 the Teller–Redlich product rule is very closely satisfied.

THE RAMAN SPECTRUM OF AMMONIA IN AQUEOUS SOLUTION

The aqueous solution (28%) of ammonia was contained in a Wood-type Raman tube, 2 cm. in diameter, with an illuminated section 60 cm. long. Two straight water-cooled mercury lamps were used for illumination and a sheet of aluminum foil was wrapped around the system to form a light furnace. The spectrograph employed was a two-prism glass instrument of the Littrow type with a reciprocal linear dispersion of 10 cm.$^{-1}$ per mm. at 4358 Å. With a spectral slit width of 2 cm.$^{-1}$ the spectrum was photographed in an exposure time of 16 hr. on Eastman 103a0 plates.

The spectrum showed three maxima at measured Raman displacements 3222, 3309, and 3398 cm^{-1}. No fine structure could be observed on the spectrogram or on the microphotometer tracing. Since the dispersion of the spectrograph was considerably greater than had been employed in the earlier investigations and the slit width much less than the line spacing reported by Langseth and by Hollaender and Williams, it was concluded that the fine structure measured by these authors was spurious. There is no doubt that the three maxima observed in the aqueous solution should be assigned to $2\nu_4$, ν_1, and ν_3 as in the liquid and solid. The polarization measurements by Marchand (11) for the solution are in accordance with this assignment.

The Raman displacements as obtained in this investigation for ammonia in the condensed phases are summarized in Table I along with the data for the

TABLE I

THE HIGHER FREQUENCY RAMAN DISPLACEMENTS OF AMMONIA

State	Density (Amagat units)	$2\nu_4$ (cm.$^{-1}$)	ν_1 (cm.$^{-1}$)	ν_3 (cm.$^{-1}$)
Gas	3	3219	3334	3444
Liquid	865	3218	3300	3373
Solid	1000	3220	3265	3365
Aqueous solution (28%)	325 (NH_3) +700 (H_2O)	3222	3309	3398

low pressure gas. Densities measured in Amagat units, which are a measure of the molecular density, are also given in the table. It is interesting to note that the frequency change in both ν_1 and ν_3 in passing from the gas to the liquid or solid is considerably greater than in passing to the aqueous solution, even though the molecular density (ammonia + water) is higher in the latter and the dipole moment of the water molecule is greater than that of the ammonia molecule. This observation indicates that the dielectric properties of the surrounding medium are not the only factors determining the frequency change, and that for polar molecules the possibility of a resonance interaction between vibrating dipoles is of comparable significance.

ACKNOWLEDGMENT

This research was supported in part by a grant from the National Research Council of Canada.

REFERENCES

1. ANDRYCHUK, D. Ph.D. Thesis, University of Toronto, Toronto, Ont. 1948.
2. BHAGAVANTAM, S. Indian J. Phys. 5: 54. 1930.
3. CRAWFORD, M. F., WELSH, H. L., and HARROLD, J. H. Can. J. Phys. 30: 81. 1952.
4. CUMMING, C. and WELSH, H. L. J. Chem. Phys. 21: 1119. 1953.
5. DAURE, P. Ann. phys. 12: 375. 1929.
6. DAURE, P., KASTLER, A., and BERRY, H. Compt. rend. 202: 569. 1936.
7. HOLLAENDER, A. and WILLIAMS, J. W. Phys. Rev. 42: 379. 1932.
8. LANGSETH, A. Z. Physik, 77: 60. 1932.
9. LEWIS, C. M. and HOUSTON, W. V. Phys. Rev. 44: 903. 1933.
10. MACNAUGHTON, E. B. Ph.D. Thesis, University of Toronto, Toronto, Ont. 1948.
11. MARCHAND, A. Compt. rend. 232: 396. 1951.
12. REDING, F. P. and HORNIG, D. F. J. Chem. Phys. 19: 594 1951.
13. SUTHERLAND, G. B. B. M. Proc. Roy. Soc.(London), A, 141: 535. 1933.

SOME EXPERIMENTS AND THEORETICAL CONSIDERATIONS ON THE ELECTRIC H.F.S. METHOD OF NUCLEAR ALIGNMENT[1]

By J. M. Daniels

ABSTRACT

An account is given of two unsuccessful experiments to detect a nuclear electric quadrupole splitting in a solid by essentially thermal methods. In one experiment *p*-diiodobenzene was mixed with potassium chromium alum and cooled to 0.01°K. by adiabatic demagnetization, in an attempt to find the nuclear specific heat of the iodine. In another experiment, a single crystal of cobalt *p*-toluenesulphonate containing some I^{131} as *p*-iodobenzenesulphonate was cooled by adiabatic demagnetization, in an attempt to produce an alignment of the I^{131} nuclei and hence an anisotropic distribution of the emitted γ-rays.

This is followed by a theory of the relaxation time for the transfer of heat from an assembly of nuclei with a quadrupole splitting to an assembly of paramagnetic ions in the same crystal. The behavior of the relaxation time is discussed with regard to variations of external magnetic field, and replacement of the nuclei or the paramagnetic ions with inert entities. A numerical estimate is made of the relaxation time of cobalt/zinc *p*-bromobenzenesulphonate for cobalt concentrations of 100% and 1%. The result of the two experiments is discussed in relation to the theory. An extension of the Casimir and du Pré relations to cover this case is given.

I. INTRODUCTION

In many substances, some of the atomic nuclei are subject to interactions between their electric quadrupole moments and the electric field gradient produced by their surrounding electrons. This causes a splitting of the $(2I+1)$-fold degenerate nuclear ground state (where I is the nuclear spin) which should give rise to a Schottky type anomaly in the specific heat, and in suitable cases lead to alignment of the nuclei at low enough temperatures (13). Neither of these effects has yet been observed in cases where this is the only interaction between a nucleus and its surrounding electrons. The principal difficulty is that such effects would be apparent only at temperatures below 0.1°K., and at these temperatures the relaxation time for the transfer of energy from the nuclear spins is usually much longer than the time available for experiment. For example, Heitler and Teller (9) estimated relaxation times as long as years for the transfer of heat from the nuclear spins to the lattice vibrations in dielectric substances at these temperatures. Observed nuclear spin – lattice relaxation times are considerably shorter than these, and it was shown by Rollin and Hatton (14) that infinitesimal quantities (i.e. 1 in 10^6) of paramagnetic impurities shorten the nuclear spin – lattice relaxation times to the order of minutes, by providing an alternative path for heat transfer from the nuclei to the lattice.

Now at these low temperatures, any heat reservoir would consist of an assembly of paramagnetic ions whose temperature has been lowered by adiabatic demagnetization. If this is to be used to cool an assembly of nuclei, one route for the transfer of the heat from the nuclei to the ions is via the

[1]*Manuscript received May 3, 1954.*
Contribution from the Department of Physics, University of British Columbia, Vancouver, B.C.

lattice. This process, involving nuclear spin – lattice and ionic spin – lattice relaxation and also lattice conductivity, is necessarily a slow one, and is the only one where the paramagnetic ions and the assembly of nuclei are contained in different chemical substances. It seems therefore more logical and desirable to cut out this slow process by finding a substance which contains both the nuclei of interest and the paramagnetic ions for cooling, as suggested by Pound (13). The nuclei and the ions, being in close proximity, would be expected on the basis of the experiments of Rollin and Hatton (14) to interact relatively strongly through magnetic dipole coupling, and thus rapid heat transfer would be favored.

The purpose of this paper is to present the results of some theoretical considerations and some experimental investigations of this idea. This work is, as yet, incomplete, but the results so far obtained are considered sufficiently interesting to warrant preliminary publication. The work is described in chronological, rather than logical, order.

II. SOME EXPERIMENTS

(*a*) *On p-Diiodobenzene.—An Attempt to Observe the Nuclear Specific Heat*

At the suggestion of Professor Pound, we made a mixture of potassium chromium alum and *p*-diiodobenzene in the proportions of one atom of iodine to each chromic ion. The mixture was compressed in a pill press at 20 tons/sq. in., and the resulting cylinder turned on a lathe to the shape of a prolate spheroid. This composite specimen was cooled by adiabatic demagnetization, and the subsequent course of the magnetic susceptibility (and hence the temperature of the potassium chromium alum) was observed. The entropy – absolute temperature relation for potassium chromium alum has been recently redetermined by Daniels and Kurti (6) with this experiment in view, and the entropy–temperature relation for the Schottky anomaly due to the iodine can be easily calculated, provided the splittings are known. Table I gives values of the entropy of the Schottky anomaly; the splitting parameter ϵ/k assumed was 0.012°K. This was later found to be within 10% of the true value, according to unpublished resonance measurements by B. V. Rollin.

Several demagnetizations from an H/T value of 15,000 gauss/°K. resulted in a final absolute temperature of 0.011°K., the value to be expected for potassium chromium alum alone. If there had been good thermal contact between the iodine nuclei and the chromic ions, the temperature to be expected after demagnetization (as calculated from the entropy values just mentioned) would have been 0.022°K. That this was not observed indicates that the relaxation time for the transfer of heat from the iodine nuclei to the chromic ions is longer than the time for demagnetization. If the relaxation time were of the order of a few minutes, two things would be expected:

(i) Immediately after demagnetization a fairly rapid heating of the chrome alum to approximately 0.028°K., due to transfer of heat from the iodine nuclei to the chromic ions.

(ii) After irradiation with γ-rays, the temperature of the chrome alum might under certain circumstances decrease, since the chrome alum has more elec-

trons per chromic ion than the *p*-diiodobenzene has per iodine nucleus. The alum could therefore warm up faster than the *p*-diiodobenzene on account of its higher γ-ray absorption, and be subsequently cooled by the latter.

Neither of these effects was observed. In fact the composite specimen behaved exactly like ordinary potassium chromium alum. We therefore conclude that the time for heat transfer from the iodine nuclei to the chrome alum is too long for our experiments. This is just what Professor Pound had suspected from his resonance measurements. It is conceivable that irradiation of the *p*-diiodobenzene with γ-rays, the normal method of heating at low temperatures, might have produced paramagnetic crystal defects (e.g. *F*-centers) at least temporarily and hence have shortened the spin–lattice relaxation time; but if this happened, its effect was insufficient to be noticed.

TABLE I

THE ENTROPY OF THE SCHOTTKY ANOMALY CAUSED BY THE QUADRUPOLE SPLITTING OF I^{127} IN TERMS OF THE SPLITTING PARAMETER ϵ
$\pm\frac{5}{2}$ LEVEL LOWEST—CALCULATED FROM THE PARTITION FUNCTION $1+e^{-2\epsilon/kT}+e^{-3\epsilon/kT}$

ϵ/kT	$S/R-\ln 2$	ϵ/kT	$S/R-\ln 2$
0	$\ln 3=1.0986$	1.00	0.5244
0.1	1.0906	1.25	0.3656
0.2	1.0662	1.50	0.2470
0.3	1.0221	1.75	0.1631
0.4	0.9717		
0.5	0.9060	2.00	0.1070
		2.25	0.0695
0.6	0.8323	2.50	0.0442
0.7	0.7542	2.75	0.0239
0.8	0.6750		
0.9	0.5976	3.00	0.0185

(*b*) *On Cobalt p-Iodobenzenesulphonate.—An Attempt to Produce Nuclear Alignment*

In the search for a substance which contains not only covalently bonded iodine but also paramagnetic ions, we were led to consider the salts of *p*-iodobenzenesulphonic acid. The salts of most of the divalent metals of the iron group with benzenesulphonic acid, *p*-toluenesulphonic acid, and the *p*-halogenbenzenesulphonic acids form isomorphous crystals. These crystals are monoclinic, but the clinic angle is between 91° and 94°; hence to a first approximation they can be considered orthorhombic. Their external morphology has been described by various authors (7, 1, 12, 17). The crystal structure of four of them has been determined by X-rays: zinc and magnesium benzenesulphonate by Broomhead and Nicol (4), and zinc and magnesium *p*-toluenesulphonate by Hargreaves (8). If the crystal structure is assumed to be the same as that evaluated in detail for the benzenesulphonates, there are two dissimilar iodine nuclei per unit cell, and the carbon–iodine bonds each make an angle of about 12° with the crystallographic *a*-axis. The salts crystallize easily from water, and in this respect are similar to the Tutton salts. They are also similar to the Tutton salts in their magnetic properties.* A single crystal

**I am indebted to Dr. K. D. Bowers of the Clarendon Laboratory, Oxford, for making some preliminary paramagnetic resonance measurements on this substance.*

was grown with the formula $(8\%\ Co/92\%\ Zn)(p.CH_3.C_6H_4.SO_3)_2.6H_2O$ in which a few of the methyl groups were replaced by iodine containing about 12 μcuries of I^{131}. Most of the cobalt was replaced by zinc in order to reduce interactions, and hence to facilitate the attainment of a low temperature on demagnetization. I^{131} was obtained as a solution of carrier free iodide ion from A.E.R.E., Harwell, and was introduced as follows. A few milligrams of the sodium salt of sulphanilic acid were diazotized with sodium nitrite and hydrochloric acid, and the iodine was added along with twice the stoichiometric quantity of potassium iodide to act as carrier. The mixture was allowed to stand for a few hours at room temperature, and was then boiled. In this reaction (Sandmeyer's reaction) iodine replaces the amino group to give *p*-iodobenzenesulphonic acid. A few drops of hydrogen peroxide were added to decompose the unchanged iodide into free iodine, which was then extracted with carbon tetrachloride. The mixture was then boiled to decompose the unreacted hydrogen peroxide, and to expel the remaining carbon tetrachloride; and, when cool, was added to the solution of cobalt and zinc *p*-toluenesulphonates.

The crystal was cooled by adiabatic demagnetization from a field of 15,000 gauss/degree applied along the crystallographic *c*-axis. Such an H/T value is sufficient to magnetize the salt to about 98% of saturation. On demagnetization, there should be produced a considerable alignment of the iodine nuclei along the crystallographic *a*-axis, and hence some of the radiations from the I^{131} might be expected to become anisotropic in their angular distribution. The decay scheme of I^{131} is not yet fully known, and there are two possible schemes to choose from (10, 11). It was thought possible that either or both of the 364 kev. and the 638 kev. γ-rays might show some anisotropy, and hence the γ-radiation from the crystal was observed along the crystallographic *a* and *b* axes with scintillation counters adjusted to count γ-rays of energy greater than 350 kev.

The ratio of the counting rates along the *a* and *b* axes after demagnetization was the same within 1% as at higher temperatures. This negative result may be explained by the observation that, according to susceptibility measurements along the crystallographic *c*-axis of the specimen, the temperature did not fall below 0.1°K. This is about three times as large as was expected, and no measurable nuclear alignment could reasonably be expected at this temperature. It may be that, although cobalt *p*-iodobenzenesulphonate is a desirable substance for the mechanics of nuclear alignment, there is unfortunately a large amount of exchange interaction between the cobalt ions, and such a possible explanation cannot be ruled out.

After these two negative results, further experiments on these lines were postponed in favor of other more immediately productive research.

III. DERIVATION OF A FORMULA FOR ESTIMATING THE NUCLEAR–IONIC RELAXATION TIME

The nuclei, which are subject to the quadrupole interaction, and the paramagnetic ions are supposed to be fixed on definite lattice points. We shall consider the energy levels of the whole lattice of nuclei and paramagnetic ions (hereafter called the crystal) in the absence of dipole coupling between the

nuclei and the ions, and shall regard this coupling as a perturbation. Time dependent perturbation theory will be used to calculate the transitions between the energy levels of the crystal, and hence to evaluate the nuclear–ionic relaxation time.

Assume that each nucleus has two levels of energy 0 and ϵ of degeneracy D_0 and D_ϵ respectively, as determined by the quadrupole interaction. The interaction between the nuclei will be considered too small to affect appreciably the energy eigenstates of the nuclei, but strong enough to ensure thermal equilibrium in the assembly of nuclei. Let T_n be the temperature of the assembly of nuclei.

Before applying the perturbation procedure, we should know the zero order states for the crystal; and for these we require to know also the energy eigenstates of the assembly of ions under the influence of their own interactions (and in the presence of an external magnetic field, if one be applied). Such eigenstates are not known in detail. They will be represented only symbolically here, since it will be shown that it is not necessary to know them in detail in order to estimate the relaxation time. Since the energy levels of such a strongly interacting assembly are almost so numerous as to form a continuum, let us assume that they do form a continuum, and that in the range E to $E+dE$ there are $\rho(E).dE$ energy levels. Let T_e be the temperature of the assembly of ions.

Let $|E, \epsilon\rangle$ denote a state of total energy $E+\epsilon$, where the ions are in a state of energy E and the assembly of nuclei consists of one nucleus in a state of energy ϵ.* To the first order in perturbation, transitions will take place to states in the neighborhood of $|E+\epsilon, 0\rangle$, and the a-priori probability per second of such a transition is

$$[1] \qquad (2\pi/\hbar)\ \rho(E+\epsilon)\ D_0 |\langle E, \epsilon|\mathfrak{H}|E+\epsilon, 0\rangle|^2$$

where $\mathfrak{H}$ is the nuclear–ionic interaction Hamiltonian. Thus the a-priori probability per unit time of a transition from a state in the neighborhood of $|E, \epsilon\rangle$ to one in the neighborhood of $|E+\epsilon, 0\rangle$ is

$$(2\pi/\hbar)\ \rho(E)\ \rho(E+\epsilon)\ D_0 D_\epsilon |\langle E, \epsilon|\mathfrak{H}|E+\epsilon, 0\rangle|^2 dE.$$

Now the occupation numbers of states $|E, \epsilon\rangle$ and $|E+\epsilon, 0\rangle$ are respectively

$$e^{-E/kT_e}\, e^{-\epsilon/kT_n}/Z_e(D_0+D_\epsilon\, e^{-\epsilon/kT_n})$$

and

$$e^{-(E+\epsilon)/kT_e}/Z_e(D_0+D_\epsilon\, e^{-\epsilon/kT_n})$$

where Z_e is the partition function for the assembly of ions. Thus the actual transition probability per second from a state near $|E, \epsilon\rangle$ to one near $|E+\epsilon, 0\rangle$ is

**Strictly we should consider the totality of nuclear states. E.g. if there are M nuclei, there are levels of the assembly of nuclei which have energy $n\epsilon$ and are $D_\epsilon{}^n\ D_0{}^{M-n}\ M!/n!(M-n)!$-fold degenerate. But since the dipolar interaction Hamiltonian $\mathbf{s}.\mathbf{I}/r^3-3(\mathbf{s}.\mathbf{r})(\mathbf{I}.\mathbf{r})/r^5$, which describes the interaction between a nucleus and an ion, is linear in the nuclear spin $\mathbf{I}$, only one nucleus turns over at a time, and the final result is the same as is obtained by considering an "assembly" of one nucleus, as is done in the text. The treatment in the text is algebraically simpler, and hence less obscure.*

$$\frac{e^{-E/kT_e}\, e^{-\epsilon/kT_n} - e^{-(E+\epsilon)/kT_e}}{Z_e(D_0+D_e\, e^{-\epsilon/kT_n})} \frac{2\pi}{\hbar}\, \rho(E)\, \rho(E+\epsilon)\, D_0 D_e |\langle E, \epsilon|\mathfrak{H}|E+\epsilon, 0\rangle|^2 dE.$$

Putting $T_n \simeq T_e = T$, $T_n - T_e = \delta T$, and summing the result over all energy values E, the total transition probability per second, W, from a nuclear state $|\epsilon\rangle$ to one $|0\rangle$ becomes:

[2]

$$W = \frac{2\pi}{\hbar}\frac{\epsilon}{k}\frac{\delta T}{T^2}\frac{D_0 D_e\, e^{-\epsilon/kT}}{Z_e(D_0+D_e\, e^{-\epsilon/kT})}\int_{-\infty}^{+\infty} \rho(E)\, \rho(E+\epsilon)\, e^{-E/kT} |\langle E, \epsilon|\mathfrak{H}|E+\epsilon, 0\rangle|^2 dE.$$

Now if an assembly of several nuclei is considered, and not just one nucleus as hitherto, the heat transferred per second from the assembly of nuclei to the assembly of ions is $\epsilon\sum_j W_j$ where W_j is the value of W for the j-th nucleus. Hence

[3] $$\frac{d}{dt}\delta T = -\frac{1}{C_n}\left(1+\frac{C_n}{C_e}\right)\epsilon \sum_j W_j$$

where C_n and C_e are the specific heats of the assemblies of nuclei and ions respectively. Since each W_j is linear in δT, equation [3] can be compared with the standard relaxation equation $d(\delta T)/dt = -\delta T/\tau$ which defines the relaxation time τ. Putting $\lambda = 1+C_n/C_e$ and

$$C_n = MD_0D_e\, e^{-\epsilon/kT}\, \epsilon^2/kT^2(D_0+D_e\, e^{-\epsilon/kT})^2,$$

the Schottky value, where M is the total number of nuclei, and substituting these values into equations [2] and [3], we find

[4] $$\frac{1}{\tau} = \frac{2\pi}{\hbar}\frac{(D_0+D_e\, e^{-\epsilon/kT})}{Z_e}\frac{\lambda}{M}\int_{-\infty}^{+\infty}\rho(E)\rho(E+\epsilon)e^{-E/kT}\sum_j |\langle E,\epsilon|\mathfrak{H}_j|E+\epsilon,0\rangle|^2 dE.$$

Now substitute for $\mathfrak{H}_j$ the expression

$$g\beta\gamma\beta_N\sum_i\left\{\frac{\mathbf{s}_i.\mathbf{I}_j}{r_{ij}^3} - 3\frac{(\mathbf{s}_i.\mathbf{r}_{ij})(\mathbf{I}_j.\mathbf{r}_{ij})}{r_{ij}^5}\right\},$$

the value of the interaction energy for the case where all the ions have the same isotropic gyromagnetic ratio g. β and β_N are the Bohr magneton and the nuclear magneton respectively, and γ is the nuclear gyromagnetic ratio. $\mathbf{s}_i$ is the spin operator for the i-th ion, $\mathbf{I}_j$ is the nuclear spin operator for the j-th nucleus, and $\mathbf{r}_{ij}$ is the distance between the i-th ion and the j-th nucleus. The integrand in [4] then becomes

[5] $$g^2\beta^2\gamma^2\beta_N{}^2\rho(E)\rho(E+\epsilon)e^{-E/kT}\sum_j\left\{\langle\epsilon|I_{jx}|0\rangle\sum_i\frac{r_{ij}{}^2-3x_{ij}{}^2}{r_{ij}{}^5}\langle E|S_{ix}|E+\epsilon\rangle\right.$$
$$-3\sum_i\frac{y_{ij}z_{ij}}{r_{ij}{}^5}(\langle\epsilon|I_{jy}|0\rangle\langle E|S_{iz}|E+\epsilon\rangle+\langle\epsilon|I_{jz}|0\rangle\langle E|S_{iy}|E+\epsilon\rangle)$$
$$\left.+\text{ similar terms in } y \text{ and } z\right\}^2.$$

We can treat in a similar way the problem of absorption of energy by the assembly of paramagnetic ions from an alternating magnetic field. If an

alternating magnetic field of peak magnitude H_1 and frequency ν such that $h\nu = \epsilon$ is applied along the x-axis, the rate of absorption of energy κ_x by the ions* from the alternating field is given by:

$$[6] \qquad \kappa_x = \frac{\pi g^2\beta^2 H_1^{\,2}}{2\hbar}\,\epsilon\,\frac{1-e^{-\epsilon/kT}}{Z_e}\int_{-\infty}^{+\infty}\rho(E)\rho(E+\epsilon)e^{-E/kT}\left|\sum_i \langle E|S_{ix}|E+\epsilon\rangle\right|^2 dE.$$

In equations [5] and [6] there are a large number of matrix elements of the type $\langle E|S_{ix}|E+\epsilon\rangle$ and $\langle\epsilon|I_{jx}|0\rangle$. The energy eigenvalue (E, ϵ, etc.) is not sufficient to specify these states completely, and hence the symbols for the matrix elements do not necessarily each represent a unique number. For example, if $I = 3/2$ and if the electric field gradient has axial symmetry so that I_z is a good quantum number, the states $|\epsilon\rangle$ and $|0\rangle$ are doublets spanned by $I_z = \pm 3/2$ and $I_z = \pm\frac{1}{2}$ respectively. Thus $\langle\epsilon|I_x|0\rangle$ can take the values $\frac{1}{2}\sqrt{3}$ and 0 for $\langle\frac{3}{2}|I_x|\frac{1}{2}\rangle$ and $\langle\frac{3}{2}|I_x|-\frac{1}{2}\rangle$ respectively, and other values if the symbols $|\epsilon\rangle$ and $|0\rangle$ represent mixtures of the appropriate basic states. But in these transitions I_z changes by only one unit, hence the value $\frac{1}{2}\sqrt{3}$ should be used for $\langle\epsilon|I_x|0\rangle$. More complicated cases can be similarly treated, and it is easily seen that the appropriate value for $\langle\epsilon|\mathbf{I}|0\rangle$ is the root mean square of all the matrix elements of this type in any representation.

The case of elements of the type $\langle E|S_{ix}|E+\epsilon\rangle$ is rather more complicated, for not only is there the possibility of uncertainties similar to those for the nuclear matrix elements if the states $|E\rangle$ and $|E+\epsilon\rangle$ are degenerate, but also the value of an element $\langle E|S_{ix}|E+\epsilon\rangle$ between unambiguous states $|E\rangle$ and $|E+\epsilon\rangle$ depends strongly on the particular ion i. In order to progress further, let us make the assumption that, given any E and $E+\epsilon$,

$$\left|\sum_i \langle E|S_{ix}|E+\epsilon\rangle\right|^2 \simeq \sum_i |\langle E|S_{ix}|E+\epsilon\rangle|^2.$$

Such an assumption may be made plausible by consideration of the following extreme cases.

(a) In an assembly of ions where there is a large external magnetic field but no interionic interaction, and $\epsilon = g\beta H_0$, all matrix elements of this type are zero, except for one. Hence

$$\left|\sum_i \langle E|S_{ix}|E+\epsilon\rangle\right|^2 = \sum_i |\langle E|S_{ix}|E+\epsilon\rangle|^2.$$

(b) If there is no external magnetic field, but strong interionic interaction, we may consider that, for the majority of states, individual ions execute incoherent precession. It might therefore be reasonable to assume that for any pair of states $|E\rangle$ and $|E+\epsilon\rangle$ but for different values of i, matrix elements of the type $\langle E|S_{ix}|E+\epsilon\rangle$ have randomly distributed phases, and some definite distribution of magnitudes. The operation of evaluating $\sum_i \langle E|S_{ix}|E+\epsilon\rangle$ is then the same as performing a random walk in the Argand diagram. In this case $|\sum_i \langle E|S_{ix}|E+\epsilon\rangle|^2$ may take a variety of values, but the average value is $\frac{1}{2}\sum_i |\langle E|S_{ix}|E+\epsilon\rangle|^2$. Now in the derivation of equation [1], it is assumed that the square modulus of the matrix element is a slowly varying function of

*If the crystal is subjected to an alternating field of this frequency, there will be also a strong resonant absorption by the nuclei. This is in addition to the absorption κ by the ions alone.

energy E (15). This may not be so if the phases of the matrix elements $\langle E|S_{ix}|E+\epsilon\rangle$ are also randomly distributed for a definite i and different states $|E\rangle$ and $|E+\epsilon\rangle$. Hence it is appropriate to replace $|\sum_i \langle E|S_{ix}|E+\epsilon\rangle|^2$ by its average value $\frac{1}{2}\sum_i |\langle E|S_{ix}|E+\epsilon\rangle|^2$.

It is seen that the value of $|\sum_i \langle E|S_{ix}|E+\epsilon\rangle|^2$ in (a) is twice that in (b); in a calculation of this type a factor $\frac{1}{2}$ is unimportant. Equation [6] now becomes

$$[7]\quad \kappa_x \simeq \frac{\pi g^2\beta^2 H_1^{\,2}}{2\hbar}\,\epsilon\,\frac{1-e^{-\epsilon/kT}}{Z_e}\int_{-\infty}^{+\infty}\rho(E)\rho(E+\epsilon)e^{-E/kT}\sum_i |\langle E|S_{ix}|E+\epsilon\rangle|^2 dE.$$

The double sum in equation [5] can be written in tensor notation

$$\sum_j \left|\sum_i A_{ij\alpha\beta}S_{i\alpha}I_{j\beta}\right|^2$$

where $S_{i\alpha}$ and $I_{j\beta}$ stand respectively for $\langle E|S_{i\alpha}|E+\epsilon\rangle$ and $\langle\epsilon|I_{j\beta}|0\rangle$, α and β are free indices indicating the coordinates x, y, z, and $A_{ij\alpha\beta}$ is the tensor $(1-3x_{ij\alpha}x_{ij\beta}/r_{ij}^2)/r_{ij}^3$. In the absence of an external magnetic field, making the assumption of random phases as before, we have for the most probable value of this sum

$$\sum_j\sum_i |S_{i\alpha}|^2|A_{ij\alpha\beta}I_{j\beta}|^2.$$

We can invert the order of this sum, and if the crystal structure is such that all the nuclei are in equivalent positions, each factor $\sum_j |A_{ij\alpha\beta}I_{j\beta}|^2$ is independent of i. The double sum then becomes

$$[8]\quad \sum_i |S_{ix}|^2\sum_j |A_{ijx\beta}I_{j\beta}|^2+\sum_i |S_{iy}|^2\sum_j |A_{ijy\beta}I_{j\beta}|^2+\sum_i |S_{iz}|^2\sum_j |A_{ijz\beta}I_{j\beta}|^2$$

The other extreme case, where there is a large external magnetic field, can be similarly treated. In this case, we have a knowledge of the states of the ionic assembly, and proceeding as before, we find that the double sum in [5] reduces to an expression like [8] except that the lattice sums (i.e. terms like $\sum_j |A_{ij\alpha\beta}I_{j\beta}|^2$) are different. These lattice sums depend on the relative orientations of the axes of the crystal, the external field, and the electric field gradient, but are not so different from those in [8] to make an enormous difference to the order of magnitude of the relaxation time when finally calculated. There seems to be no point in pursuing them in detail at this stage.

When expression [8] is substituted into equations [4] and [5], the integral in equation [4] is a linear combination of those in [7]. These integrals can thus be eliminated, and we find, for the zero field case, that

$$[9]\quad \frac{1}{\tau} = \frac{D_0+D_\epsilon e^{-\epsilon/kT}}{1-e^{-\epsilon/kT}}\,\frac{8\gamma^2\beta_N^{\,2}}{\epsilon}\,\frac{\lambda}{M}\left(\sum_j |A_{ijx\beta}I_{j\beta}|^2\frac{\kappa_x}{H_1^{\,2}}+\sum_j |A_{ijy\beta}I_{j\beta}|^2\frac{\kappa_y}{H_1^{\,2}}+\sum_j |A_{ijz\beta}I_{j\beta}|^2\frac{\kappa_z}{H_1^{\,2}}\right).$$

IV. APPLICATION TO THE COBALT *p*-HALOGENBENZENESULPHONATES

Since the detailed crystal structure is unknown, we will assume a representative simplified structure, viz.: the unit cell is orthorhombic with $a = 25.9$Å, $b = 6.38$Å, $c = 6.95$Å; there are two cobalt ions in the unit cell at $(0, 0, 0)$ and $(\frac{1}{2}, \frac{1}{2}, \frac{1}{2})$, and four halogen nuclei at $(\frac{1}{8}, 0, 0)$, $(\frac{3}{8}, \frac{1}{2}, \frac{1}{2})$, $(\frac{5}{8}, \frac{1}{2}, \frac{1}{2})$, and

$(\frac{7}{8}, 0, 0)$. Assume that the axis of the electric field gradient coincides with the crystallographic a-axis for each halogen nucleus. We shall consider the cobalt ions as having an isotropic $g = 3$ and no h.f.s.

Let us now assume that we are dealing with a bromobenzenesulphonate where $I = 3/2$, since this case fits the simple theory just given. Then $D_0 = D_\epsilon = 2$ and $(D_0+D_\epsilon e^{-\epsilon/kT})/(1-e^{-\epsilon/kT}) \rightarrow 2$ as $T \rightarrow 0$ and $\rightarrow kT/2\epsilon$ as $T \rightarrow \infty$. We will assume that the specific heat of the assembly of ions is much greater than that of the nuclei, and hence $\lambda = 1$. If this is not so, the relaxation time will turn out to be shorter than calculated. Also $M = 2N$, since there are twice as many halogen nuclei as ions. With these substitutions, expression [9] for the relaxation time becomes at low temperatures

$$[10] \quad \frac{1}{\tau} = \frac{8\gamma^2\beta_N{}^2}{\epsilon}\left[\frac{3}{4}\left\{\sum_j\left(\frac{r_{ij}{}^2-3x_{ij}{}^2}{r_{ij}{}^5}\right)^2+9\sum_j\frac{x_{ij}{}^2y_{ij}{}^2}{r_{ij}{}^{10}}\right\}\frac{\kappa_x}{NH_1{}^2}\right.$$
$$\left. + \text{ two similar terms obtained by permuting } x, y, \text{ and } z\right].$$

If we assume that $\kappa_x = \kappa_y = \kappa_z$, put $\epsilon = 0.012$ cm.$^{-1}$, and take the magnetic moment of the bromine nucleus to be 2.17 nuclear magnetons, an average for the two isotopes, [10] becomes:

$$[11] \quad 1/\tau = 121\times10^{16}\,\kappa/NH_1{}^2.$$

The difficulty now is to estimate the quantity $\kappa/NH_1{}^2$, and this is especially difficult since relatively little is known about the shapes of paramagnetic resonance absorption lines. The assumptions which have to be made are rather arbitrary, and the final value obtained for τ depends greatly on what is assumed for κ. For this reason, there is little point in making a detailed numerical calculation, and the result evaluated for cobalt p-bromobenzenesulphonate could apply equally well to cobalt p-iodobenzenesulphonate. The problem of determining κ has been treated by several authors, e.g. Broer (3) who deals particularly with the case where there is zero external field. If we assume, as he does, that an appropriate expression for κ in this case is

$$\kappa/H_1{}^2 = K\nu^2e^{-\nu^2/2\nu_0{}^2}$$

where ν_0 is a characteristic (spin–spin relaxation) frequency for the assembly of ions, and insert numerical values into his formulae, we find the results given in Table II.

TABLE II

CALCULATIONS OF RELAXATION TIMES FOR (Co/Zn)(p.Br.$C_6H_4.SO_3)_2.6H_2O$

% Co sites occupied	ν_0	ν/ν_0	τ at high temp. (sec.)	τ at low temp. (sec.)
100%	2×10^9	0.18	5×10^{-5}	$0.008\,T$
1%	2×10^8	1.8	2×10^{-4}	$0.04\,T$

V. DISCUSSION OF THE FORMULAE FOR THE RELAXATION TIME

The formula given in equation [9] has been obtained using many assumptions which should strictly be justified in detail, e.g.:

(i) That there is separate thermal equilibrium in the nuclear and ionic assemblies.

(ii) That the establishment of equilibrium between the two assemblies is slower than the establishment of thermal equilibrium in either assembly.

(iii) That the square modulus of a sum of matrix elements of the type encountered is approximately equal to the sum of their square moduli.

(iv) That it is permissible to take a function which fits the shape of a paramagnetic absorption line near resonance and to extrapolate this function into its "tail" and expect the result to represent the nonresonant absorption there.

(v) That the direct (first order) process treated here is more important than the Raman (second order) process. If this is not so, the final result for τ will be too high.

Despite the questionable nature of these assumptions, it was thought desirable to carry out some calculation based on them in order to obtain guidance about what might be expected in the real case. In any case, it is possible to make qualitative if not quantitative deductions about the behavior of τ.

The factors which tend to promote a short relaxation time, besides large nuclear and ionic moments and short distances between nuclei and ions, are those which tend to increase κ; i.e. a suitable distribution of energy levels of the ionic assembly. Both for large κ and short τ, it is necessary to have a large number of pairs of ionic energy levels separated by an energy gap ϵ, and between which transitions are allowed. In a magnetically dilute crystal, where the ions are without either Stark or hyperfine splittings, it is likely that the most numerous of such pairs of energy levels will lie one in each tail of the level distribution $\rho(E)$ and hence τ will be comparatively large. Stark and hyperfine splittings, and also interionic interactions, tend to spread out the distribution of energy levels and hence favor a short τ. This is especially effective if there are pairs of energy levels for an isolated ion which are separated by ϵ. This might arise if a hyperfine splitting of each ion fortuitously happens to be equal to ϵ, or if a suitable external magnetic field is applied to give a Zeeman splitting equal to ϵ. In the case of the simplified model of cobalt *p*-bromobenzenesulphonate, this field is of the order of 100 gauss. Under these conditions of "resonant relaxation" assumptions (i) and (ii) are certainly invalid, and all that can be said is that τ is very short. If the ions have a fine structure, or a hyperfine structure, there may be several relaxation resonances.

The dependence of τ on temperature, by equation [9], follows from the temperature dependence of κ and $(D_0+D_\epsilon e^{-\epsilon/kT})/(1-e^{-\epsilon/kT})$. If the ionic assembly is paramagnetic, and the line shape is independent of temperature, $\kappa \propto 1/T$ and hence τ is independent of T at high temperatures, and proportional to T at low temperatures.* Further inspection of equation [9] indicates that τ is independent of the nuclear concentration, when some of the nuclear sites

**It might not be out of place to emphasize here exactly what is meant by high and low temperatures in this context. "High temperatures" means the range, say, from 0.03°K. to 1°K. in the salt under discussion; i.e. high compared with the characteristic temperature of the hyperfine structure Schottky anomaly, yet low enough so that lattice vibrations, which have been ignored in the theory, can be safely ignored. "Low temperatures" mean, conversely, temperatures low compared with the characteristic temperature of the hyperfine structure Schottky anomaly, yet still high enough for the lattice of ions to be paramagnetic as is assumed in the theory. It is evident that in many cases, such a low temperature region may not exist.*

are randomly occupied by entities which take no part in this process (e.g. nuclei of spin zero). The dependence of τ on ionic concentration under similar circumstances (e.g. when cobalt is replaced randomly by zinc) is governed by the dependences of the paramagnetic (i.e. ionic) absorption κ, *per cubic centimeter*, on concentration. Variation of the ionic concentration alters not only the number of ions per cubic centimeter available to absorb radiation, but also in general alters the shape of the absorption line, and both these effects have to be considered.

When we consider the results for cobalt *p*-bromobenzenesulphonate in Table II, it would seem that the values of τ calculated for the 100% and 1% cobalt concentrations are reasonable, especially since the real cobalt ion has an extensive hyperfine splitting which has been ignored in the calculation and which certainly helps to shorten τ. If this calculation is applied to salts with a much smaller cobalt concentration, ridiculously long relaxation times result. For example, times of the order of 10^{70} sec. are calculated for a cobalt concentration of 0.01%. This is quite out of accord with the experience of Rollin and Hatton (14), and indicates that the theory is inadequate in this case for various reasons. Among these is undoubtedly that the assumed Gaussian line shape is incorrect in this case (assumption iv), and that other effects assume greater prominence. A discussion of possible alternative mechanisms for relaxation in very dilute paramagnetics has been given by Bloembergen (2). In the experiment described in II(*b*), it seems almost inconceivable that the iodine nuclei were not cooled, since on demagnetization, the external magnetic field must have passed through a relaxation resonance at some time.

VI. A POSSIBLE METHOD OF OBSERVING THE NUCLEAR–IONIC RELAXATION TIME DIRECTLY

If the crystal is placed in an alternating magnetic field of frequency $\simeq 1/\tau$, there should be absorption of energy due to the nuclear–ionic relaxation mechanism, just as there is for spin–lattice relaxation. The extension of the well-known theory of Casimir and du Pré (5) is straightforward. Assume that the assembly of ions can exchange energy with the lattice with a relaxation time τ', and with the nuclei with a relaxation time τ, but that the nuclei cannot exchange energy with the lattice. Let u be the ratio of the specific heat of the ionic assembly to the specific heat of the nuclear assembly, and let χ_T and χ_S be respectively the isothermal and adiabatic susceptibilities of the ionic assembly. Then the complex susceptibility χ of the ionic assembly at an angular frequency ω is given by

$$\chi = \chi_T - (\chi_T - \chi_S) \Big/ \left(1 + \frac{1}{i\omega\tau'} + \frac{1}{u + i\omega\tau}\right).$$

If $\tau \ll \tau'$, two relaxation regions are seen, and a mechanism like this could explain the "intermediate relaxation phenomenon" of de Vrijer and Gorter (16).

ACKNOWLEDGMENTS

The experimental part of this work was carried out at the Clarendon Laboratory, Oxford, and I am indebted to Professor Lord Cherwell for extend-

ing to me the facilities of his laboratory. I am also indebted to Dr. N. Kurti and Mr. F. N. H. Robinson, for assistance with the experimental work, to Dr. P. F. D. Shaw for assistance with chemical matters, to Dr. M. A. Grace who maintained the nuclear physics equipment, and to Prof. R. V. Pound for many helpful discussions.

The theoretical investigation of the experiments was carried out at the University of British Columbia, where I am grateful for the interest shown in this work by Dr. W. Opechowski and Dr. G. M. Volkoff.

REFERENCES

1. ARMSTRONG, H. E. and RODD, E. H. Proc. Roy. Soc. (London), A, 90: 463. 1914.
2. BLOEMBERGEN, N. Physica, 15: 386. 1949.
3. BROER, L. J. F. Physica, 10: 801. 1943.
4. BROOMHEAD, J. M. and NICOL, A. D. I. Acta Cryst. 1: 88. 1948.
5. CASIMIR, H. B. G. and DU PRÉ, F. K. Physica, 5: 507. 1938.
6. DANIELS, J. M. and KURTI, N. Proc. Roy. Soc. (London), A, 221: 243. 1954.
7. GROTH, P. Chemische Kristallographie. Bd. IV. Verlag von Wilhelm Engelmann, Leipzig. 1917.
8. HARGREAVES, A. Nature, 158: 620. 1946.
9. HEITLER, W. and TELLER, E. Proc. Roy. Soc. (London), A, 115: 629. 1936.
10. KERN, B. D., MITCHELL, A. G. C., and ZAFFARANO, D. J. Phys. Rev. 76: 94. 1949.
11. METZGER, F. and DEUTSCH, M. Phys. Rev. 74: 1610. 1948.
12. MUMMERY, C. S. Proc. Roy. Soc. (London), A, 90: 455. 1914.
13. POUND, R. V. Phys. Rev. 70: 1410. 1949.
14. ROLLIN, B. V. and HATTON, J. Phys. Rev. 74: 346. 1948.
15. SCHIFF, L. I. Quantum mechanics. 1st ed. McGraw-Hill Book Company, Inc., New York. 1949. p. 193.
16. DE VRIJER, F. W. and GORTER, C. J. Physica, 18: 549. 1952.
17. WEIBULL, R. Z. Krist. 15: 235. 1889.

NOTE

A LOGARITHMIC PHOTOMETER

By H. L. Grant and R. W. Stewart

INTRODUCTION

In some optical experiments it is necessary to measure a very wide range of intensities, but only to an accuracy of the order of 25%. This was the case recently when the problem was to measure the luminous flux passing through a surface as a function of distance along the surface, assuming that this flux was a function of one dimension of the surface only. The ratio of maximum to minimum intensity was as much as 300 : 1, so a logarithmic scale was obviously desirable.

It has long been known (1) that the distance of penetration of light into an opalescent material is a logarithmic function of the intensity incident upon the surface. It can be shown (see Appendix) that this logarithmic relation holds if some of the light is allowed to escape from the side of the material, and that the distribution of this escaping light can be used as a measure of the depth of penetration.

For the type of measurement indicated above, it is necessary to prevent the light from spreading sideways. This can be done well enough by constructing a "sandwich" consisting of layers of $\frac{1}{8}$ in. opalescent plexiglas separated by sheets of polished foil or shimstock. Such a sandwich is shown in Fig. 1. The dimensions of the plastic elements are $\frac{1}{8}$ in. $\times \frac{1}{4}$ in. $\times 3$ in. and the back of the sandwich is of polished aluminum so that no light is lost in that direction.

CALIBRATION AND USE OF SANDWICH

The depth of penetration of light has been measured by photographing the illuminated sandwich and making a print on high contrast paper. It is then quite easy to measure the depth by choosing the point at which the graininess disappears into the white of the overexposed region or into the blackness of the underexposed region. The latter method is less reliable unless it is certain that no stray light is falling on the front face of the sandwich when it is being photographed.

The calibration was carried out by illuminating the edge of the sandwich with a point source at various distances to give an intensity range of 400 to 1. The average distance of penetration for three representative elements is shown as a function of the logarithm of intensity in Fig. 3. Only one point has fallen more than 10% in intensity from the best straight line. The slope of the curve, $d(\log_{10} I)/dx$, is equal to 1.08 cm^{-1}. Average figures have been plotted because of the small scatter between individual points. This is illustrated in Table I.

Fig. 2 shows the instrument illuminated by an uneven intensity distribution, and Fig. 4 is the resulting graph.

There is no apparent reason why the calibration curve could not be extrapolated in the high intensity direction to the extent of at least another factor

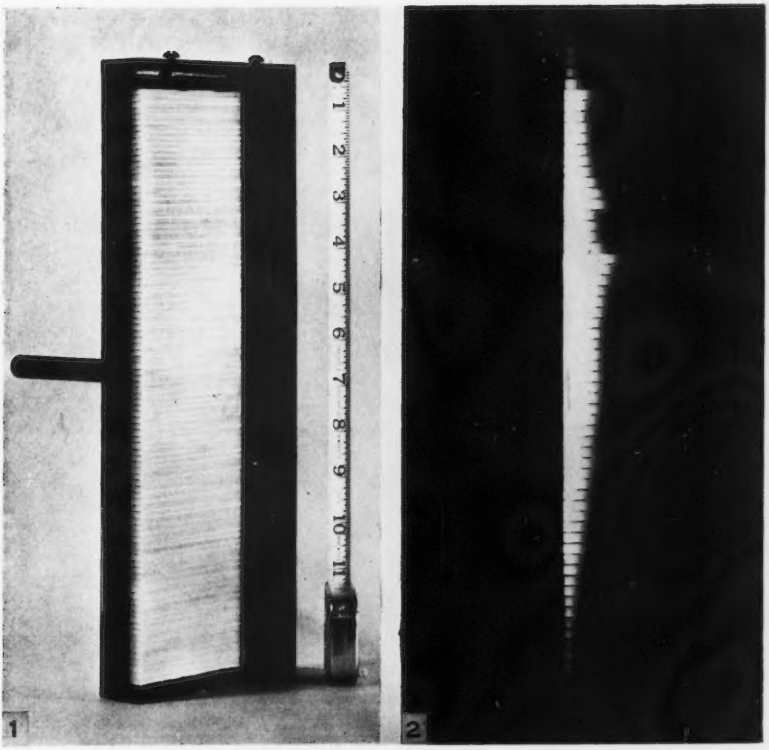

FIG. 1. The photometer sandwich.
FIG. 2. Photograph of the photometer sandwich when illuminated by an uneven intensity distribution.

TABLE I

DISTANCE OF PENETRATION FOR THREE DIFFERENT ELEMENTS IN CENTIMETERS

$\log_{10}$(Intensity)	Element		
	A	*B*	*C*
5.00	2.82	2.72	2.74
4.77	2.60	2.60	2.58
4.54	2.34	2.33	2.25
4.40	2.24	2.24	2.17
4.20	2.09	2.04	2.01
4.00	1.79	1.79	1.77
3.80	1.66	1.64	1.61
3.60	1.42	1.42	1.42
3.40	1.25	1.26	1.24
3.20	1.10	1.07	1.08
3.00	0.86	0.86	0.86
2.80	0.71	0.76	0.71
2.60	0.59	0.62	0.58
2.40	0.39	0.41	0.37

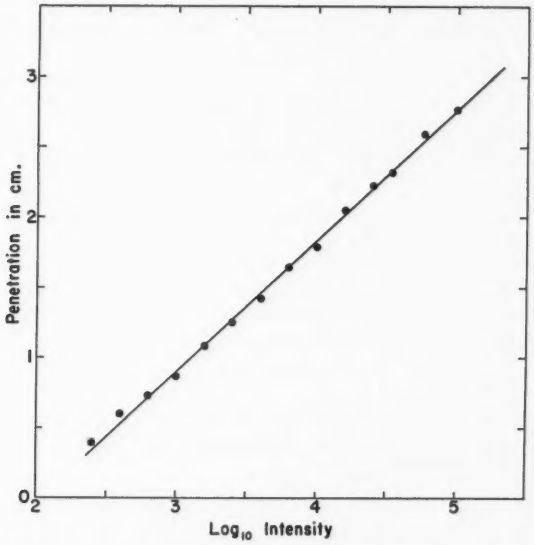

FIG. 3. Calibration curve, showing the average distance of penetration for three representative elements. Figures for individual elements are given in Table I.

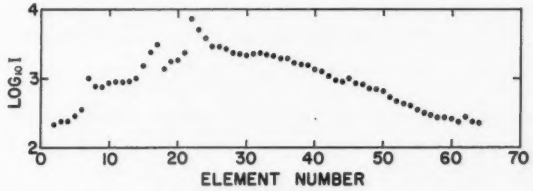

FIG. 4. The intensity curve obtained from Fig. 2.

of 10. The calibration was not extended because the extra intensity was not readily available and the extra range was not needed for our work. It would also appear possible to make an absolute calibration if it were required.

For intensity distributions of this type, the photometer sandwich has proved to be a reliable and simple device for making a quick intensity measurement simultaneously at many points along a line. The individual elements could, if desired, be made to present a much smaller area to the incident light.

1. CHANNON, H. J., RENWICK, F. F., and STORR, B. V. Proc. Roy. Soc.(London), A, 94: 222. 1918.

APPENDIX

Propagation of Light in a Strip of the Plastic

Light in opalescent plexiglas appears to suffer multiple scattering, the path between scatterers being small compared with the dimensions of the sandwich. The problem is therefore one of diffusion with absorption.

Let ϕ = energy density, i.e. the light energy per unit volume. The rate of diffusion of a quantity across a surface is proportional to the component of the gradient normal to the surface. In this case, the energy crossing per unit time is

$$\nu \, \partial\phi/\partial n$$

where $\partial\phi/\partial n$ is the component of the gradient normal to the surface and ν is a diffusion constant. By considering a volume element, dx, dy, dz, and noting that the net luminous flux into the element must be equal to that lost by absorption, we obtain

$$[1] \qquad \nabla^2\phi = (\sigma/\nu)\phi$$

where σ is the absorption per unit time per unit volume.

Let us take a co-ordinate system in the sandwich such that the aluminum back is in the x-z plane and the illuminated edge in the y-z plane.

If the brass spacers are perfectly reflecting, we have

$$\partial\phi/\partial z = 0$$

within one plastic strip if it is uniformly illuminated at the end (which we shall assume). The problem is then two dimensional and the boundary conditions are:

$$(a) \quad \partial\phi/\partial y = 0 \text{ when } y = 0,$$

$$(b) \quad \partial\phi/\partial y = -k\phi \text{ when } y = a,$$

where $y = a$ is the equation of the front face and k is a constant related to the reflectivity of this face;

$$(c) \quad \phi \text{ and all its derivatives vanish when } x = \infty,$$

$$(d) \quad \phi = f(y) \text{ when } x = 0.$$

$f(y)$ will be left an arbitrary function at this stage. There is no simple general solution satisfying these boundary conditions unless k is very large or very small with respect to unity.

If, however, $f(y) = A \cos \alpha y$, where α is the solution of the transcendental equation $\alpha = k \cot \alpha a$, then

$$\phi = A \cos \alpha y \exp -(\alpha^2+\sigma/\nu)^{\frac{1}{2}}x \qquad [2]$$

and the amount of light leaving the front face will vary as $\exp -(\alpha^2+\sigma/\nu)^{\frac{1}{2}}x$.

For any other function $f(y)$, the scale will not be a simple logarithmic one in x, but the other terms will again be of exponential form, decaying more rapidly than $\exp -(\alpha^2+\sigma/\nu)^{\frac{1}{2}}x$ as x increases so that at sufficiently large x the intensity curve will approximate equation [2]. In practice, it has been found satisfactory to leave the end of the element unshaded.

Received June 23, 1954.
Pacific Naval Laboratory,
Defence Research Board,
H.M.C. Dockyard,
Esquimalt, B.C.

LETTERS TO THE EDITOR

Under this heading brief reports of important discoveries in physics may be published. These reports should not exceed 600 words and, for any issue, should be submitted not later than six weeks previous to the first day of the month of issue. No proof will be sent to the authors.

Three-quantum Annihilation of Positrons in Solids*

Bell and Graham (1) have shown that positrons entering metals and crystalline solids annihilate with mean lives near 2×10^{-10} sec. Their experiments also showed that positrons entering certain non-crystalline materials have a complex time decay; about two thirds annihilating with a short (about 3×10^{-10} sec.) mean life and the remaining one third annihilating with a mean life of about 2×10^{-9} sec. The fraction of positrons that decay by the long lifetime process appears to be independent of the material. It was postulated (1) that the long lifetime is due to the formation of triplet positronium atoms which can then decay by either of two modes, viz., by ordinary three-quantum decay or by conversion to the singlet state followed by two-quantum decay. Since the lifetime of the free triplet atoms is much longer, 1.4×10^{-7} sec. (3, 4), than the observed lifetime, one would conclude that most ($\simeq 99\%$) of the triplet atoms decay via the conversion ${}^3S \rightarrow {}^1S$ process.** Hence the fraction of triplet positronium atoms that decay by the three-quantum process should be proportional to the long lifetime.

This letter reports measurements of the number of three-quantum decays in various substances. The experimental arrangement was similar to that used by DeBenedetti and Siegel (2) but had a 10^{-8} sec. triple coincidence circuit. The positron source (Na^{22}) was made by evaporating a sodium chloride solution on 2 mgm./cm.^{2} aluminum foil and covering with another layer of the same foil. Measurements were made by sandwiching this source between layers of the specimen material.

The data are presented in Table I and Fig. 1. The mean lifetimes for positron annihilation in some of these materials (1) are included for comparison. The errors shown in the table

TABLE I

OBSERVED THREE-QUANTUM DECAY RATES IN CONDENSED MATERIALS

Material	Three-quantum rate at 20°C. (counts/min.)	Positron mean lives (1) (sec.) 1	2
Lithium	0.15 ± 0.05	$(1.5 \pm 0.6) \times 10^{-10}$	—
Beryllium	0.14 ± 0.05	$(1.7 \pm 0.5) \times 10^{-10}$	—
Aluminum	0.20 ± 0.05	$(1.5 \pm 0.3) \times 10^{-10}$	—
Copper	0.16 ± 0.05	$(1.2 \pm 0.5) \times 10^{-10}$	—
Gold	0.13 ± 0.05	$(1.2 \pm 0.3) \times 10^{-10}$	—
Lead	0.11 ± 0.05	$(1.5 \pm 0.6) \times 10^{-10}$	—
Uranium	0.16 ± 0.05	Not measured	Not measured
Urea	0.21 ± 0.07	Not measured	Not measured
Rubber (pure gum)	0.20 ± 0.07	Not measured	Not measured
Crystalline quartz	0.22 ± 0.05	$(2.0 \pm 0.3) \times 10^{-10}$	—
Fuzed quartz	0.41 ± 0.10	$(3.5 \pm 0.5) \times 10^{-10}$	$(1.8 \pm 0.2) \times 10^{-9}$
Polystyrene	0.47 ± 0.12	$(3.7 \pm 0.5) \times 10^{-10}$	$(2.3 \pm 0.2) \times 10^{-9}$
Teflon	0.68 ± 0.10	Not measured	$(3.5 \pm 0.4) \times 10^{-9}$

indicate the reproducibility of results throughout the course of the experiment and are larger than statistical counting errors. These results show that crystalline quartz and metals, for which no second lifetime was observed, have similar low three-quantum decay rates, while materials which show the long lifetime have higher rates of three-quantum decay. The variation of three-quantum decay rate in teflon was measured as a function of temperature. The results of this experiment are shown in the figure. A correlation between the longer lifetimes and the three-quantum annihilation rates is readily seen.

To obtain a quantitative measure of the relative three-quantum rates in different substances allowance would have to be made in the above data for positrons which annihilate in the relatively thick source materials. It was not possible to determine accurately the amount to be subtracted but experiments indicated that it would be an appreciable fraction of the rate

**Issued as A.E.C.L. No. 132.*

A preliminary report of this work was given at the May 1953 Meeting of the Canadian Association of Physicists, in London, Ontario.

***Pond (5) observes a similar formation of triplet positronium in gases which can decay by conversion to the singlet state followed by two-quantum annihilation.*

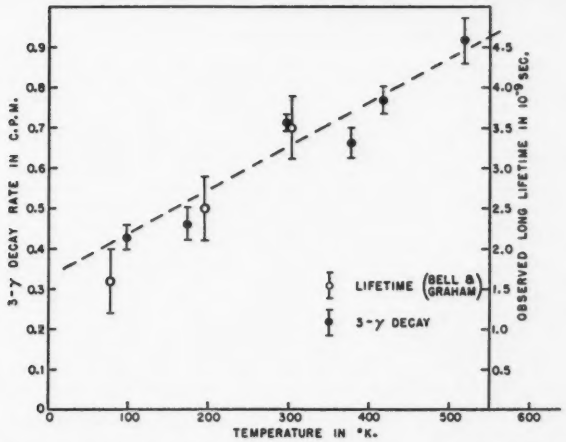

FIG. 1. Three-quantum annihilation rate of positrons in teflon as a function of temperature. The dashed line is a least squares fit of these data. For comparison the lifetime measurements of Bell and Graham are also shown. Standard deviations are shown by vertical bars.

observed in metals. Further experiments are planned which we expect will establish a quantitative correlation between the longer mean lifetimes and the three-quantum annihilation rates.

It is a pleasure to thank Mr. R. M. MacIntyre for assistance with some of the experiments. We are indebted to Prof. M. Deutsch who kindly sent us a Na^{22} positron source.

1. BELL, R. E. and GRAHAM, R. L. Phys. Rev. 90: 644. 1953.
2. DEBENEDETTI, S. and SIEGEL, R. Phys. Rev. 85: 371. 1952; 94: 955. 1954.
3. DEUTSCH, M. Phys. Rev. 83: 866. 1951. SHEARER, J. W. and DEUTSCH, M. Phys. Rev. 76: 462. 1949.
4. ORE, A. and POWELL, J. L. Phys. Rev. 75: 1696. 1949.
5. POND, T. A. Phys. Rev. 85: 489. 1952.

RECEIVED AUGUST 6, 1954.
PHYSICS DIVISION,
ATOMIC ENERGY OF CANADA LIMITED,
CHALK RIVER, ONTARIO.

R. L. GRAHAM
A. T. STEWART

CANADIAN JOURNAL OF PHYSICS

Notes to Contributors

Manuscripts

(i) ***General.*** Manuscripts should be typewritten, double spaced, on paper 8½×11 in. **The original and one copy are to be submitted.** Tables (each typed on a separate sheet) and captions for the figures should be placed at the end of the manuscript. Every sheet of the manuscript should be numbered.

Style, arrangement, spelling, and abbreviations should conform to the usage of this journal. Names of all simple compounds, rather than their formulas, should be used in the text. Greek letters or unusual signs should be written plainly or explained by marginal notes. Superscripts and subscripts must be legible and carefully placed.

Manuscripts should be carefully checked before they are submitted; authors will be charged for changes made in the proof that are considered excessive.

(ii) ***Abstract.*** An abstract of not more than about 200 words, indicating the scope of the work and the principal findings, is required, except in Notes.

(iii) ***References.*** References should be listed **alphabetically by authors' names,** numbered, and typed after the text. The form of the citations should be that used in this journal; in references to papers in periodicals, titles should not be given and only initial page numbers are required. All citations should be checked with the original articles and each one referred to in the text by the key number.

(iv) ***Tables.*** Tables should be numbered in roman numerals and each table referred to in the text. Titles should always be given but should be brief; column headings should be brief and descriptive matter in the tables confined to a minimum. Numerous small tables should be avoided.

Illustrations

(i) ***General.*** All figures (including each figure of the plates) should be numbered consecutively from 1 up, in arabic numerals, and each figure referred to in the text. The author's name, title of the paper, and figure number should be written in the lower left corner of the sheets on which the illustrations appear. Captions should not be written on the illustrations (see Manuscript (i)).

(ii) ***Line Drawings.*** Drawings should be carefully made with India ink on white drawing paper, blue tracing linen, or co-ordinate paper ruled in blue only; any co-ordinate lines that are to appear in the reproduction should be ruled in black ink. Paper ruled in green, yellow, or red should not be used unless it is desired to have all the co-ordinate lines show. All lines should be of sufficient thickness to reproduce well. Decimal points, periods, and stippled dots should be solid black circles large enough to be reduced if necessary. Letters and numerals should be neatly made, preferably with a stencil (**do NOT use typewriting**), and be of such size that the smallest lettering will be not less than 1 mm. high when reproduced in a cut 3 in. wide.

Many drawings are made too large; originals should not be more than 2 or 3 times the size of the desired reproduction. In large drawings or groups of drawings the ratio of height to width should conform to that of a journal page but the height should be adjusted to make allowance for the caption.

The original drawings and one set of clear copies (e.g. small photographs) are to be submitted.

(iii) ***Photographs.*** Prints should be made on glossy paper, with strong contrasts. They should be trimmed so that essential features only are shown and mounted carefully, with rubber cement, on white cardboard.

As many photographs as possible should be mounted together (with a **very** small space between each photo) to reduce the number of cuts required. Full use of the space available should be made and the ratio of height to width should correspond to that of a journal page; however, allowance must be made for the captions. Photographs or groups of photographs should not be more than 2 or 3 times the size of the desired reproduction.

Photographs are to be submitted in duplicate; if they are to be reproduced in groups one set should be mounted, the duplicate set unmounted.

Reprints

A total of 50 reprints of each paper, without covers, are supplied free. Additional reprints, with or without covers, may be purchased.

Charges for reprints are based on the number of printed pages, which may be calculated approximately by multiplying by 0.6 the number of manuscript pages (double-spaced typewritten sheets, 8½ × 11 in.) and making allowance for illustrations (not inserts). The cost per page is given on the reprint requisition which accompanies the galley.

Any reprints required in addition to those requested on the author's reprint requisition form must be ordered officially as soon as the paper has been accepted for publication.

Contents

Printed in Canada *by* University of Toronto Press